The export of African mineral dust across the Atlantic and its impact over the Amazon Basin

Xurong Wang[1,2,a,+], Qiaoqiao Wang[1,2,+], Maria Prass[3], Christopher Pöhlker[3], Daniel Moran-Zuloaga[3], Paulo Artaxo[4] Jianwei Gu[5], Ning Yang[1,2], Xiajie Yang[1,2], Jiangchuan Tao[1,2], Juan Hong[1,2], Nan Ma[1,2], Yafang Cheng[3], Hang Su[3], Meinrat O. Andreae[3,6]

[1.] Institute for Environmental and Climate Research, Jinan University, Guangzhou, 511443, China

[2.] Guangdong-Hongkong-Macau Joint Laboratory of Collaborative Innovation for Environmental Quality, Guangzhou, 511443, China

[3.] Multiphase Chemistry Department, Max Planck Institute for Chemistry, Mainz, 55128, Germany

[4.] Institute of Physics, University of São Paulo, São Paulo, 05508-900, Brazil

[5.] Institute of Environmental Health and Pollution Control, School of Environmental Science and Engineering, Guangdong University of Technology, Guangzhou, 510006, China

[6.] Scripps Institution of Oceanography, University of California, San Diego, CA 92093-0230, USA

[a.] now at: Atmospheric Chemistry Department, Max Planck Institute for Chemistry, Mainz, 55128, Germany

[+.] These authors contribute equally to this article

Correspondence to, Qiaoqiao Wang (qwang@jnu.edu.cn)

Abstract

The Amazon Basin is frequently influenced by the trans-Atlantic transport of African dust plumes during ~~the~~its wet season~~,~~ (January – April), which not only interrupts the near-pristine atmospheric condition in that season, but also provides nutrient inputs into the Amazon rainforest ~~associated with dust deposition. The factors controlling the long-range transport (LRT) of African dust towards the Amazon Basin and consequently the overall impact of African dust over the Amazon Basin are not yet well understood.~~upon deposition. In this study, we use the chemical transport model GEOS-Chem to investigate the impact of the export of African mineral dust ~~upon~~to the Amazon Basin during the period of 2013 – 2017, constrained by multiple datasets obtained from AERONET, MODIS, as well as Cayenne site and the Amazon Tall Tower Observatory (ATTO) site in the Amazon Basin. With optimized particle mass size distribution (PMSD~~),~~) of dust aerosols, the model well captures observed AOD regarding both the mean value as well as the decline rate of the logarithm of AOD over the Atlantic Ocean along the transport path (AOaTP), implying the consistence

with observed export efficiency of African dust along the trans-Atlantic transport. With an annual emission of 0.73 ± 0.12 Pg ~~a~~yr^{-1}, African dust entering the Amazon Basin has surface concentrations of 5.7 ± 1.3 µg m^{-3} (up to 15 µg m^{-3} in the northeast corner) during the wet season, accounting for ~~47% ±~~ $40\% \pm 4.$5.~~0~~% (up to 70%) of mass concentrations of total aerosols. Observed dust peaks over the Amazon Basin are generally associated with relatively higher African dust emissions (including Sahara and Sahel) and longer lifetime of dust along the trans-Atlantic transport, namely higher export efficiency of African dust across the Atlantic Ocean. The frequency of dust events in the Amazon Basin in the wet season is around 18% averaged over the basin, with maxima over 60% at the northeast coast. During the dust events, AOD over most of the Amazon Basin is dominated by dust. ~~Observed peaks of African dust over the Amazon Basin are generally associated with relatively higher African dust emissions and longer lifetime of dust along the trans-Atlantic transport, namely higher export efficiency of African dust across the Atlantic Ocean.~~ Associated with dust deposition, we further estimate annual inputs of 52 ± 8.7, 0.97 ± 0.16 and 21 ± 3.6 mg m^{-2} ~~a~~yr^{-1} for iron, phosphorus and magnesium deposited into the Amazon rainforest, respectively, which may well compensate the hydrologic losses of nutrients in the forest ecosystem.

1 Introduction

The desert over North Africa, being the world's largest dust source, contributes to over 50% of global dust emission (Kok et al., 2021; Wang et al., 2016). Dust particles are uplifted by strong surface winds, and then typically transported ~~westwards to the tropical~~downwind for a long distance, reaching Atlantic, Caribbean~~and~~, America, and Europe (Prospero et al., 1981; Ben-Ami et al., 2012; Yu et al., 2019; Swap et al., 1992; Prospero et al., 2014~~).~~; Wang et al., 2020). The emission varies on daily to seasonal and even decadal time scales, largely affected by local wind speed, land surface cover, soil moisture, etc (Ridley et al., 2014; Mahowald et al., 2006). Once present in the atmosphere, mineral dust can degrade air quality downwind as well as

modify the atmospheric radiative balance via directly scattering and absorbing solar radiation (Ryder et al., 2013b), and altering cloud properties by acting as cloud condensation nuclei or ice nuclei (Chen et al., 1998; Demott et al., 2003; Mahowald and Kiehl, 2003; Dusek et al., 2006). Additionally, mineral dust contains iron, phosphorous, and other nutrients, and could affect ocean biogeochemistry and fertilize tropical forest upon downwind deposition (Niedermeier et al., 2014; Rizzolo et al., 2017).

There is an increased concern about the impact of African dust exerted over the Amazon basin, which being the world's largest rainforest, represents a valuable but also vulnerable ecosystem, and is sensitive to any disturbance from climate changes associated with human activities in the future (Andreae et al., 2015; Pöhlker et al., 2019). During the wet season (January – April) Amazonian aerosols are generally dominated by local biogenic aerosol, with remarkably low PM_{10} mass concentrations of a few μg m^{-3} (Andreae et al., 2015; Martin et al., 2010a; Prass et al., 2021). The near-pristine condition, however, is frequently interrupted by the transatlantic transport of ~~Afreian~~African dust toward the Amazon Basin (Andreae et al., 2015; Martin et al., 2010b; Martin et al., 2010a; Talbot et al., 1990). The dusty episodes could drastically increase the aerosol optical depth (AOD, by a factor of 4), mass concentrations of coarse aerosol (with diameter > 1 μm~~) (~~, up to 100 μg m^{-3}), as well as crustal elements over the Amazon Basin (Ben-Ami et al., 2010; Pöhlker et al., 2019; Moran-Zuloaga et al., 2018; Baars et al., 2011; Formenti et al., 2001). Therefore, there is great interest in understanding factors controlling the export of African dust towards the Amazon Basin and the impact they might have on the environment, ecosystem, and climate.

Over the past decades, field measurements combined with satellite observation and forward/back trajectory analysis have been conducted to explore the long-range transport (LRT) of African dust toward the Amazon Basin (e.g. Ben-Ami et al., 2010; Pöhlker et al., 2018; Prospero et al., 2020). The transatlantic transport of African dust plumes is closely related to annual north-south oscillation of the intertropical

convergence zone (ITCZ) (Moran-Zuloaga et al., 2018; Ben-Ami et al., 2012),

favoring the path towards the Amazon Basin in the late boreal winter and spring

(December-April) as the ITCZ moves southward. In addition to the annual oscillation

of ITCZ, the export efficiency of African dust towards the Amazon Basin also highly

depends on the lifetime of mineral dust, which is largely affected by the

meteorological condition (e.g. precipitation). Dust particles are subject to wet removal

when they are within or underneath precipitating clouds. For instance, Yu et al. (2020)

argued that El Djouf, in western Sahara, contributes more dust to the Amazon Basin

than the Bodélé depression as the transport paths of dust released from El Djouf are

less affected by the rainy cloud.

Besides meteorological conditions, dust size distribution can also influence its

lifetime and consequently the export efficiency of African dust towards the Amazon

Basin. Previous studies have observed that volume/mass fractions of coarse mode dust

particles, giant particles in particular, tend to be reduced along the transport due to

higher gravitational settling velocities (Ryder et al., 2018; Ryder et al., 2013b; Ryder

et al., 2013a; Van Der Does et al., 2016). Moreover, the optical properties of mineral

dust are also strongly size dependent, especially for those in sub-micron range (Liu et

al., 2018; Di Biagio et al., 2019; Ysard et al., 2018). For instance, Ryder et al. (2013a)

reported a loss of $60 - 90\%$ of particles with diameter > 30 μm in size 12 h after uplift

and consequently an increase in the single scattering albedo from 0.92 to 0.95

associated with the change in the size distribution of dust aerosols. Therefore, the size

distribution of dust particles is a key factor determining the efficiency of dust

transport and consequently the environmental and climate effect of the mineral dust

downwind (Mahowald et al., 2011a; Mahowald et al., 2011b).

It is worth mentionmentioning that the LRT events bring not only mineral dust into

the Amazon Basin but also biomass burning aerosols from Africa as well as sea spray

aerosols (Wang et al., 2016; Holanda et al., 2020; Andreae et al., 1990; Talbot et al.,

1990; Ansmann et al., 2009; Baars et al., 2011), making it challenging to have a

quantitative assessment of the impact of African dust on the Amazon Basin. So far, a

few studies have attempted to quantify the impact of the LRT of African dust over the Amazon Basin, but mainly focus on dust deposition only (e.g. Yu et al., 2015a; Ridley et al., 2012; Yu et al., 2019). Estimates of annual dust deposition and dust deposition rates into the Amazon Basin exhibit a wide range (7.7-50 Tg ~~a~~yr^{-1} and 0.8-19 g m^{-2} ~~a~~yr^{-1}, respectively), attributed to the application of different methods and the intrinsic uncertainties associated with each method (Kok et al., 2021; Yu et al., 2015b; Kaufman, 2005; Swap et al., 1992). For example, the results based on Cloud-Aerosol Lidar and Infrared Pathfinder Satellite Observations (CALIPSO) is subject to the uncertainty associated with the Cloud-Aerosol Lidar with Orthogonal Polarization (CALIOP) extinction, vertical profile shape, dust discrimination, diurnal variations of dust transport as well as the below-cloud dust missed by CALIOP (Yu et al., 2015a). While models could be considered as a useful tool to comprehensively assess the transatlantic transport of African dust towards the Amazon Basin and the consequent impact over the Amazon Basin, there exist considerable differences among model results, attributed to the uncertainties associated with the dust parameterization in the model, including emission schemes, dust size distribution, dust deposition, etc (Kim et al.,2014; Huneeus et al., 2011; Mahowald et al., 2014). Observational constraints on the modelling results along the transport from source regions to receptor regions are thus ~~necessarily needed to demonstrate the model performance and~~in urgent need to accomplish a better evaluation of factors controlling the ~~variability in the~~LRT of African dust and its overall impact over the Amazon Basin~~assessment~~.

Here, we present a detailed multiyear simulation of the export of ~~Africa~~African dust across the Atlantic and ~~the~~its impact over the Amazon Basin (around 8.8 × 10^6 km^2, see ~~Fig.~~Figure 1 for defined area) during 2013 − 2017 with the GEOS-Chem (chemical transport model). The aims of this study are: (1) to evaluate the model performance ~~regarding the~~of dust simulation ~~of dust aerosols~~ including the particle mass size distribution (PMSD), optical properties, mass concentrations as well as the ~~trans-Atlantic transport~~export efficiency of African dust towards the Amazon Basin; (2) to analyze factors controlling the export of African dust towards the Amazon

5

151 Basin; and (3) to give a comprehensive examination of the impact of African dust

152 over the Amazon Basin, including surface aerosol concentrations, AOD and nutrient

153 inputs upon deposition.

154

155 ## 2　2. Methodology

156 ## 2.1　 GEOS-Chem model

157 ### 2.1.1 Model overview

158 In this study we use the GEOS-Chem model version 12.0.0 (www. geos-chem.org) to

159 perform a global aerosol simulation with a horizontal resolution of $2° \times 2.5°$. The

160 GEOS-Chem is driven by assimilated meteorological data GEOS-FP from the NASA

161 Global Modeling and Assimilation Office (GMAO) (Lucchesi, 2013) with a native

162 horizontal resolution of $0.25° \times 0.3125°$, which is then degraded to $2° \times 2.5°$ for the

163 input to GEOS-Chem. We initialize the model with a 1-year spin-up followed by an

164 aerosol simulation from 2013 to 2017.

165 The aerosol simulation is an offline simulation for aerosol tracers including mineral

166 dust in four size bins, sea salt in fine ($\leqslant$ 1 μm in diameter) and coarse (> 1 μm in

167 diameter) modes, black carbon (BC), organic aerosols (OA)), and sulfate-nitrate-

168 ammonium aerosols in fine mode ($\leqslant$ 1 μm in diameter), sea salt in both fine and

169 coarse (> 1 μm in diameter) modes, and mineral dust in four size bins covering the

170 size range of 0.2 – 12 μm in diameter. Aerosol optical properties used for aerosol

171 optical depth (AOD) calculation are mainly based on Global Aerosol Data Set

172 (Koepke et al., 1997), with modifications in aerosol size distributions (Jaeglé et al.,

173 2011; Drury et al., 2010; Wang et al., 2003a; Wang et al., 2003b), hygroscopic growth

174 factor of organic aerosols (Jimenez et al., 2009), and the refractive index of dust

175 (Sinyuk et al., 2003). AOD in the model is then calculated online at selected

176 wavelengths assuming lognormal size distributions of externally mixed aerosols and

177 accounts for hygroscopic growth (Martin et al., 2003).

178 Wet deposition in GEOS-Chem, based on the scheme of Liu et al. (2001), accounts for

179 scavenging in both convective updrafts and large-scale precipitation. Further updates

by Wang et al. (2011) are also applied, accounting for ice/snow scavenging as well as the impaction scavenging in convective updrafts. Dry deposition in the model follows the standard resistance-in-series scheme by Wesely (2007), accounting for turbulent transfer and gravitational settling (Wang et al., 1998; Zhang et al., 2001).

2.1.2 Dust emission and PMSD schemes in the model

2.2 Observations

The particle volume size distribution (PVSD) and AOD daily data (at wavelength of 675 nm) from AERONET level 2.0 (aeronet.gsfc.nasa.gov/new_web/download_all_v3_aod.html, last access on Jun. 22, 2021(Dubovik et al., 2002)) during the year of 2013 – 2017 is used in the study to evaluate dust emissions and its PMSD over the source regions in Africa. The PVSD data provided by AERONET is a column-integrated aerosol volume size distribution and with a size range of 0.05 – 15.0 µm. For comparison with model results, the PVSD data is converted to PMSD using the same densities as in the model. In addition, to minimize the influence of aerosols other than dust, only data dominated by coarse aerosol (contribution of fine aerosol to total aerosol volume < 3% or simulated dust contribution > 95%) is used for the comparison.

The study also uses observed PMSD over central Sahara during Fennec Campaign (africanclimateoxford.net/projects/fennec/, last access: 22 June 2021) for the comparison with AERONET and our model results. Aiming to investigate dust microphysical and optical properties, 42 profiles of size distribution (0.1 – 300 µm in diameter) over both the Sahara and the Atlantic Ocean, were sampled from in-situ aircraft measurements during Fennec campaign. For more detailed description of the aircraft measurements, readers are referred to Ryder et al. (2013a).

In addition, level 3 daily AOD (at wavelength of 550 nm) data from the moderate resolution imaging spectroradiometers (MODIS) installed on Terra and Aqua platforms (https://ladsweb.modaps.eosdis.nasa.gov/archive/allData/61/, last access: 22 June 2021) is applied in the study to evaluate the trans-Atlantic transport of dust plumes from Africa toward Amazon Basin. For comparison, we degraded the original

horizontal resolution of MODIS data ($1° \times 1°$) to $2° \times 2.5°$, consistent with the model outputs.

Finally, long-term aerosol measurements at the Amazon Tall Tower Observatory (ATTO, 59.0056° W, 2.1459° S, marked in Fig. 1), located in central Amazon Basin are used in the study to evaluate the influence of the long-range transport of African dust over the Amazon Basin. The ATTO site was established in 2012 for the long-term monitoring of climatic, biogeochemical, and atmospheric conditions in the Amazon rainforest. Detailed description of the site and the measurements there could be found in Andreae et al. (2015). In this study, we only use the particle number size distribution from a Optical Particle Sizer (OPS, TSI model 3330; size range of 0.3 – 10 μm in diameter, divided into 16 size bins) and a Scanning Mobility Particle Sizer (SMPS, TSI model 3080, St. Paul, MU, USA; size range of 10 – 430 nm in diameter, divided into 104 size bins) over the period from 2014 to 2016. The number size distribution is converted to mass concentrations assuming spherical particles with a constant density of 1.5 g cm^{-3} (Pöschl et al., 2010). In addition, daily PM$_{10}$ mass concentrations during wet season (from January to April) in 2014 measured at Cayenne, French Guiana (4.9489° N, 52.3097° W, located in the northeast coast of the Amazon Basin, marked in Fig. 1, https://doi.org/10.17604/vrsh-w974) are also used in this study to further evaluate the model performance regarding the trans-Atlantic transport of African dust toward the Amazon basin. The measurement at Cayenne site is carried out on a cooperative basis by personnel of ATMO-Guyane, a non-profit organization (https://www.atmo-guyane.org/qui-sommes-nous/statuts/). The PM$_{10}$ samples are measured by a Taper Element Oscillating Microbalance (TEOM, model 1400 series, ThermoFisher Scientific) and then are returned to Miami for analysis (Prospero et al., 2020). Readers are referred to Prospero et al. (2020) for detailed description of the site and the data.

3 Dust emissions and size distribution

3.1 Dust emissions

The emission of mineral dust is based on the dust entrainment and deposition (DEAD) mobilization scheme of Zender et al. (2003) in the GEOS-Chem model ~~(Duncan Fairlie et al., 2007). Figure 1 shows the spatial distribution of simulated dust emissions and Table 1 lists seasonal and annual dust emissions in northern Africa (17.5° W − 40° E, 10° N − 35° N) for the period of 2013 − 2017. Simulated annual dust emission from northern Africa is 0.73 ± 0.12 Pg a^{-1}, contributing more than 70% of the global dust emission (0.99 ± 0.20 Pg a^{-1}). The result is in the range of $0.42 − 2.05$ Pg a^{-1} reported by Kim et al.~~ . The DEAD scheme calculates the total vertical dust flux based on the total horizontal saltation flux (Q_s) using the theory of White (1979). The Q_s depends mainly on the surface wind friction velocity and the threshold friction velocity, which is determined by soil type, soil moisture content, and surface roughness. For more details of the DEAD scheme, readers are referred to Duncan Fairlie et al. (2007). ~~(2014), who evaluated five AeroCom II global models regarding the dust simulation over similar regions.~~

~~There exists a strong seasonality in the dust emission from northern Africa, peaking in spring and winter (up to 1.2 Pg a^{-1}) and reaching the minimum in fall (around 0.33 Pg a^{-1}) in general. Previous studies have also pointed out that dust emissions over different African regions show distinct variations (Bakker et al., 2019; Shao et al., 2010), attributed to differences in geographical properties (Knippertz et al., 2007), vegetation cover (Mahowald et al., 2006; Kim et al., 2017), and meteorological mechanisms on a local scale (Alizadeh-Choobari et al., 2014; Wang et al., 2017; Roberts and Knippertz, 2012). Consequently, there exists substantial seasonal change in dust source regions. For instance, during boreal winter, the Bodélé Depression in northern Chad is found to be the most active triggered by the Harmattan winds, while the northwestern African dust sources become less active in contrast with the condition in boreal summer (Ben-Ami et al., 2012; Prospero et al., 2014). Therefore, we further analyze the emission variability over five different source regions in northern Africa (Fig. 1 and Table S1). On an annual basis, the contribution to total northern African dust emission is the largest from Region A (west Sahara, 36% ±~~

4.0%), followed by Region D (central Sahel including Bodélé, 21% ± 4.7%), Region B (central Sahara, 13% ± 2.6%), Region C (east Sahara, 12% ± 1.0%), and Region E (west Sahel, 6.5% ± 0.64%). The emission fluxes, however, are the most intensive in Region D, up to 11 ± 2.1 g month^{-1} m^{-2} and are generally below 5 g month^{-1} m^{-2} over the other regions. Concerning the seasonality, higher dust emission tends to occur in boreal spring and winter, with the largest emission flux of 19 ± 4.7 g month^{-1} m^{-2} from Region D. As shown in Fig. 2 and S1, the emissions peak in boreal spring for Region A, B and C, but in winter for Region D and E. There is also a secondary peak in summer emissions for Region E. Correlation analysis between dust emissions and meteorological variables suggests that the seasonality is mainly driven by high surface wind speeds (with r of 0.79-0.96 and 0.68-0.97 for the 75th and 95th percentiles of wind speeds, respectively). Apparent negative correlation is also found between precipitation (soil moisture, Fig. S2) and dust emission in Region D with r of -0.69 (-0.67). Similar seasonality is also reported by Cowie et al. (2014), who suggested that the strongest dust season in winter in central Sahel is driven by strong harmattan winds and frequent Low level Jet breakdown, and the second peak in summer in west Sahel could be explained by the summer monsoon combined with the Sahara Heat Low. The study also suggested the dominance of strong wind frequency in the seasonal variation of the emission frequencies.

There is a significant decrease in the annual emission from 0.88 Pg a^{-1} in 2013 to 0.56 Pg a^{-1} in 2017. Similarly, studies on African dust variability at decadal and longer time scales also reported an obviously decreasing trend in both dust emissions in Africa and dustiness over the east mid-Atlantic in recent decades since the early 1980s (Ridley et al., 2014; Middleton, 2019; Shao et al., 2013). Evan et al. (2016) pointed out three periods of persistent anomalously low dust concentrations in the 1860s, 1950s and 2000s. Weather and climate drivers behind this variability include precipitation, surface wind over northern Africa, Atlantic Multidecadal Oscillation (AMO), North Atlantic Oscillation (NAO), the movement of ITCZ, etc. For example, as shown in Fig. S2, there is an obviously increasing trend of AMO over the period

2000 – 2015, especially from 2010 to 2015 (data available from http://www.esrl.
noaa.gov, last access on July 29, 2021 (Enfield et al., 2001)). This positive AMO
phase corresponds to higher North Atlantic sea-surface temperature (SST), and could
result in enhanced rainfall in the Sahel and consequently less African dust emissions
(Middleton, 2019). A recent study by Yuan et al. (2020) projected decreased surface
wind speeds over African dust source regions as well as more precipitation in the
Sahel region due to positive interhemispheric contrast in Atlantic SST associated with
the global warming, leading to less dust emissions and weaker westward transport.
While most regions show decline trends of dust emissions, the emission in Region D
shows a slight increase. The variation is mainly associated with surface wind speeds
(Fig. S3). For instance, the 75th and 95th percentiles of wind speeds decrease by 7.0%
and 9.1% in Region B but slightly increases by 2.0% and 1.4% in Region D from
2013 to 2017. The r values are in the range of 0.90 – 0.99 between annual dust
emissions and the 95th percentile of wind speeds over all the 5 source regions.
Significant negative correlation with r of -0.52 – -0.73 between annual dust emissions
and soil moisture is also found for those regions except for Region D where r is only -
0.08.

It is also worth noting that the interannual variation in dust emission is much larger
during the wet season (0.96 ± 0.25, Table 1) than on an annual basis (0.73 ± 0.12).
Moreover, while the annual emissions gradually decrease from 2013 to 2017, the
emissions during the wet season peak in 2015. The obviously different behavior
between the annual emissions and emissions during the wet season suggests that
predictions of future impact of African dust emissions over the Amazon Basin in
response to climate change should focus on the wet season rather than the annual
average, as the former is more related to the export of African dust towards the
Amazon Basin.

**3.2 Dust size distribution and its impact on the export efficiency towards the
Amazon Basin**

325　Freshly emitted dust particles are divided into four size bins in GEOS-Chem: $0.1 -$

326　1.0 μm, $1.0 - 1.8$ μm, $1.8 - 3.0$ μm, and $3.0 - 6.0$ μm in radius. The first size bin is

327　further divided into four sub-bins ($0.1 - 0.18$ μm, $0.18 - 0.3$ μm, $0.3 - 0.6$ μm, and

328　$0.6 - 1.0$ μm in radius) for the calculation of optical properties. While total dust

329　emissions are not affected, optical properties, atmospheric lifetime and downwind

330　concentrations of dust particles are sensitive to different PMSD schemes.

331　Table 2̶1 shows 3 different PMSD schemes tested in this study: V12, V12_C and

332　V12_F. Scheme V12, which is derived based on scale-invariant fragmentation theory

333　(Kok, 2011) with modification in tunable parameters (Zhang et al., 2013), is a default

334　set in GEOS-Chem. However, this scheme has been only evaluated for US/Asian dust,

335　not for Africa. On the other hand, V12_C was used in older versions of GEOS-Chem

336　and constrained from aircraft measurements during the Saharan Dust Experiment

337　(Ridley et al., 2012; Highwood et al., 2003). In addition, we derived V12_F based on

338　the measurements during the Fennec aircraft observations also focusing on Saharan

339　dust. Among all the three PMSD, V12_C has the largest mass fraction in the first bin

340　(relatively small particles) and the lowest fraction in the last bin (large ones). In

341　contrast, V12_F has the most dust distributed in the last bin (~ 70%) and only a little

342　(around 5%) in the first bin ($0.1 - 1.0$ μm).

343　Simulated mass extinction efficiency (MEE, also shown in Table 2̶1) at wavelength of

344　550 nm for dust particles in the first sub-bin ($0.1 - 0.18$ μm) is 3.13 m^2 g^{-1},̶ and

345　decreases to 0.16 m^2 g^{-1} for those in the last bin ($3.0 - 6.0$ μm). The lifetime of dust

346　aerosols against deposition are 5.1, 2.2, 1.7 and 0.86 d in the four bins (from small to

347　large size), respectively. Therefore, ~~as mentioned before,~~ although with the same

348　emission, <u>total</u> dust AOD<u>, lifetime,</u> and <u>downwind</u> concentrations could vary greatly

349　with PMSD~~. Here~~ <u>upon emissions. In this study,</u> we <u>will</u> evaluate ~~all the~~<u>these</u> three

350　PMSD schemes <u>and the impact on AOD, dust concentrations as well as its export</u>

351　<u>efficiency along the trans-Atlantic transport from Africa to the Amazon Basin.</u>

352　**2.2 Observations**

353　<u>The study uses observations from multiple datasets obtained from AERONET,</u>

354 MODIS, as well as Cayenne site and the Amazon Tall Tower Observatory (ATTO) site

355 to constrain model results regarding the simulation of the dust export from Africa to

356 the Amazon Basin. Table 2 summarizes these observations, including the parameters,

357 the spatio-temporal coverage, and the corresponding application in the model. The

358 daily data of AOD (at wavelength of 675 nm) and particle volume size distribution

359 (PVSD) from AERONET level 2.0

360 (aeronet.gsfc.nasa.gov/new_web/download_all_v3_aod.html, last access on Jun. 22,

361 2021(Dubovik et al., 2002)) during the year of 2013 − 2017 is used in the study to

362 evaluate dust emissions and its PMSD over the source regions in Africa in the model.

363 The PVSD data provided by AERONET is a column-integrated aerosol volume size

364 distribution and with a size range of 0.05 − 15.0 μm. It is then converted to PMSD

365 using the same densities as in the model. Only sites with valid data accounting for

366 more than 30% of the total are considered in this study. In addition, to minimize the

367 influence of aerosols other than dust, only data dominated by dust (simulated dust

368 contribution to column-integrated aerosols mass concentrations > 95%) is used for the

369 comparison of PMSD. There are a few sites not far from the coast and could be

370 influenced by sea salt. With the above data screening, the sea salt contribution to total

371 aerosol mass is less than 0.5%. For the comparison of AOD, the criterion is less

372 stringent to have more data points available and uses data dominated by coarse

373 aerosols (the contribution of fine aerosol to total aerosol volume < 3%). This criterion

374 does not exclude sea salt and the contribution of sea salt to AOD could be up to 30%

375 at the Capo_Verde site (22.9° W,16.7° N) over the east of the Atlantic Ocean.

376 The study also uses observed PMSD over central Sahara during Fennec Campaign

377 (africanclimateoxford.net/projects/fennec/, last access: 22 June 2021) for the

378 comparison with AERONET and our model results. Aiming to investigate dust

379 microphysical and optical properties, 42 profiles of size distribution (0.1 − 300 μm in

380 diameter) over both the Sahara and the Atlantic Ocean, were sampled from in-situ

381 aircraft measurements during Fennec campaign. For more detailed description of the

382 aircraft measurements, readers are referred to Ryder et al. (2013a).

In addition to AERONET AOD data, level 3 daily AOD (at wavelength of 550 nm) data from the moderate resolution imaging spectroradiometers (MODIS) installed on Terra and Aqua platforms (https://ladsweb.modaps.eosdis.nasa.gov/archive/allData/61/, last access: 22 June 2021) is applied in the study to evaluate the trans-Atlantic transport of dust plumes from Africa toward Amazon Basin. For comparison, we degraded the original horizontal resolution of MODIS data ($1° \times 1°$) to $2° \times 2.5°$, consistent with the model outputs.

Finally, daily PM_{10} mass concentrations during wet season (from January to April) in 2014 measured at Cayenne, French Guiana (52.3097° W, 4.9489° N, located in the northeast coast of the Amazon Basin, https://doi.org/10.17604/vrsh-w974, marked in Figure 1) and long-term aerosol measurements at the Amazon Tall Tower Observatory, Brazil (ATTO, 59.0056° W, 2.1459° S, located in central Amazon Basin, also marked in Figure 1) are used in this study to further evaluate the model performance regarding the influence of the LRT of African dust over the Amazon Basin. The measurement at Cayenne site is carried out on a cooperative basis by personnel of ATMO-Guyane, a non-profit organization. The PM_{10} samples are measured by a Taper Element Oscillating Microbalance (TEOM, model 1400 series, ThermoFisher Scientific) and then are returned to Miami for analysis (Prospero et al., 2020). Readers are referred to Prospero et al. (2020) for detailed description of the site and the data. The ATTO site was established in 2012 for the long-term monitoring of climatic, biogeochemical, and atmospheric conditions in the Amazon rainforest. Detailed description of the site and the measurements there could be found in Andreae et al. (2015). In this study, we only use the particle number size distribution from an Optical Particle Sizer (OPS, TSI model 3330; size range of 0.3 – 10 μm in diameter, divided into 16 size bins) and a Scanning Mobility Particle Sizer (SMPS, TSI model 3080, St. Paul, MU, USA; size range of 10 – 430 nm in diameter, divided into 104 size bins) over the period from 2014 to 2016. The number size distribution is converted to mass concentrations assuming spherical particles with a constant density

14

of 1.5 g cm^{-3} (Pöschl et al., 2010).

3 Model evaluation

Here we evaluate three different PMSD schemes regarding the model performance of dust simulation through the comparison with observed mass size distribution of column-integrated aerosol over Africa, AOD over both Africa and the Atlantic Ocean, as well as PM$_{10}$ and dust concentrations in the Amazon Basin.

Figure 2 shows the mass fractions of column-integrated aerosols retrieved from AERONET sites compared with model results based on different PMSD schemes. The location of the selected AERONET sites with valid data are marked in Figure 1 as purple symbols (including asterisks and circles). The mean mass fractions for each bin from AERONET data are 17%, 27%, 38%,17%, respectively. The comparison indicates the model results based on V12_C agrees better with the observations, with much smaller mean absolute deviation (MAD) of 2.8, followed by 4.2 for V12 and 18 for V12_F. In other words, the model results with other PMSD schemes (V12_F in particular) greatly underestimate the mass fractions in the first bin and overestimate the mass fractions in the last bin. During the Fennec campaign, the aircraft sampled two strong Saharan dust outbreaks with AOD up to 1.1, which may be associated with strong winds favoring the uplift of large particles.

Figure 3 shows the times series of daily AOD at wavelength of 675 nm during the year of 2013 − 2017 from both AERONET and model results. The locations of the selected AERONET sites with valid data over northern Africa are shown in Figure 1 as purple circles. The Capo_Verde site over the east of the Atlantic Ocean is also included to show the model performance over the ocean in addition to the land. Although different PSD schemes have little influence on the correlation between AERONET and model results with most r around 0.6 − 0.7, the normalized mean bias (NMB) has been significantly improved in V12_C, with a range of -12% − 11% (vs. -33% − -11% and -42% − -19% for V12 and V12_F, respectively). The severe underestimation in AOD from V12 and V12_F could be attributed to their relatively

15

441 higher dust fractions distributed in larger size bins with lower MEE.

442 In addition, we also compare the spatial distributions of simulated AOD over the

443 Atlantic Ocean with MODIS AOD (at 550 nm) averaged over 2013 − 2017 in ~~Fig.~~

444 ~~5a~~Figure 4a-d. There is a clear decreasing trend in MODIS AOD along the trans-

445 Atlantic transport from Africa towards South America. Although all simulations show

446 similar spatial distributions with declining trends of AOD along the transport, the

447 results from V12_C are the most consistent with MODIS data with the highest *r* of

448 0.89 and the smallest NMB of 6.5% among the three schemes (vs. *r* of 0.85 and 0.81

449 and NMB of -13% and -19% for V12 and V12_F, respectively). Note that the model

450 results based on V12_C tends to overestimate MODIS AOD over Africa while no

451 significant systematic bias is found between V12_C and AERONET AOD. Wang et

452 al. (2016) sampled MODIS data at AERONET sites over Africa and found that

453 MODIS retrieval underestimate AERONET AOD at most sites with NMB of -12% − -

454 36%, which partly explain the large difference between model V12_C and MODIS

455 AOD.

456 Assuming first-order removal of aerosol along the transport, we ~~derived linear trend~~

457 ~~lines based on~~could derive the removal rates of aerosols, estimated as the gradient of

458 the logarithm of AOD (log(AOD)) against the distance over the Atlantic Ocean along

459 the transport path (AOaTP, 20° − 50° W and 5° S − 25° N, ~~Fig. 5e). MODIS AOD~~

460 ~~decrease from 0.29 ± 0.023 near the coast of Africa to 0.17 ± 0.010 at the coast of~~

461 ~~South America, with a~~Figure 4e). The decline rate of MODIS log(AOD) is 0.019 ±

462 0.0025 degree⁻¹. A similar decline rate of 0.019 ± 0.0029 degree⁻¹ is found for

463 simulated log(AOD) based on V12_C~~, decreasing from 0.28 ± 0.022 to 0.16 ± 0.013~~

464 ~~(0.019 ± 0.0029 degree⁻¹).~~. In contrast, simulations with V12 and V12_F exhibit ~~much~~

465 ~~lower AOD together with~~ relatively steeper slopes of 0.021 ± 0.0040 and 0.021 ±

466 0.0041, respectively, implying too much aerosol removal and thus lower export

467 efficiency along the transport. To specify the impact of different PMSD on the export

468 efficiency of dust aerosols towards the Amazon Basin, ~~Fig. 5f~~Figure 4f also shows

469 simulated dust AOD (DOD) along the transect from 20° to 50° W. The DOD from

16

470 V12_C decreases from 0.15 ± 0.018 to 0.049 ± 0.088 along the transport, with a

471 decreasing rate of 0.016 ± 0.0014 degree^{-1}. In contrast, DOD decreases from $0.097 \pm$

472 0.012 to 0.028 ± 0.085 with a slope of 0.018 ± 0.0016 for V12 and decreases from

473 0.080 ± 0.090 to 0.025 ± 0.084 with a slope of 0.017 ± 0.0014 for V12_F.

474 Lying in the trade wind belt, Cayenne has been taken as the gate of African dust.

475 Hence, the comparison between simulated and observed dust concentrations at

476 Cayenne site could evaluate model performance in reproducing the arrival of African

477 dust to the Amazon Basin. As shown in ~~Fig. 6a~~Figure 5a, the simulation from V12_C

478 shows excellent agreement between simulated dust and observed PM_{10} concentration

479 during wet season, with r around 0.85 and NMB of -39%. The correlation from the

480 other two simulations is similar ($r = 0.86$), but the corresponding NMB is much larger

481 (-57% for V12 and -80% for V12_F). ~~Prospero et al. (2020) did similar analysis at the~~

482 ~~Cayenne site but concerning the data all year round.~~ Based on the regression line

483 between observed concentrations of PM_{10} and dust~~, they~~ at the same site, Prospero et

484 al. (2020) obtained a regional background value of PM_{10} ranging from 17 to 22 µg m^{-}

485 ^{3}, largely attributed to sea salt aerosol, and ~~suggested~~a value of 0.9 for the slope,

486 suggesting PM_{10} values above this range as a proxy for advected dust. Consistent with

487 their results, the regression line between ~~observed PM_{10} and~~ simulated dust and PM_{10}

488 from V12_C in this study shows a background value of PM_{10} around 23 µg m^{-3}~~. The~~

489 ~~slope of the regression line from V12_C is 1.0, also consistent~~, with ~~the~~a value of ~~0.9~~

490 ~~in the study of Prospero et al. (2020), demonstrating the well performance of the~~

491 ~~model with V12_C in simulating the trans-Atlantic transport of African~~ the slope

492 around 1.0, and the dust ~~towards the Amazon Basin.~~contribution to PM_{10} is around

493 $53\% \pm 20\%$. In contrast, the regression lines from V12 and V12_F are much steeper,

494 with the slope of 1.4 and 2.1, ~~respectviely~~respectively, and the dust contributions are

495 relatively smaller, 44% in V12 and 34% in V12_F.

496 We also compare simulated dust concentrations with observed coarse particles at

497 ATTO site in central Amazon in wet season during 2014 – 2016 in ~~Fig. 6b~~Figure 5b.

498 The correlation between observed and simulated data are similar for different PMSD

schemes with r of $0.63 - 0.65$. But the bias of V12_C is negligible (NMB = -0.27%) while both V12 and V12_F tend to underestimate the coarse aerosol concentrations with NMB of -36% and -55%, respectively. The dust contribution to coarse aerosols in above 80% in V12_C, but less than 70% in V12_F. This again implies relatively higher export efficiency of African dust aerosols towards the Amazon Basin with V12_C associated with their relatively higher dust fractions distributed in smaller size bins.

Overall, compared with V12 and V12_F schemes, model results based on V12_C are more consistent with the multiple observed data sets, including column-integrated particle size distribution, AOD and surface coarse aerosol concentrations obtained either over sources or downwind of the sources. Therefore, we use the model results from V12_C (hereinafter referred to as model results unless noted otherwise) to investigate the transatlantic transport of dust from Africa and its impact over the Amazon Basin in the following sections.

4   Results and discussion

4.1 Dust emissions

Figure 1 shows the spatial distribution of simulated dust emissions and Table 3 lists seasonal and annual dust emissions in northern Africa ($17.5° W - 40° E$, $10° N - 35° N$) for the period of $2013 - 2017$. Simulated annual dust emission from northern Africa is 0.73 ± 0.12 Pg yr^{-1}, contributing more than 70% of the global dust emission (0.99 ± 0.20 Pg yr^{-1}). The result is in the range of $0.42 - 2.05$ Pg yr^{-1} reported by Kim et al. (2014), who evaluated five AeroCom II global models regarding the dust simulation over similar regions.

There exists a strong seasonality in the dust emission from northern Africa, peaking in spring and winter (up to 1.2 Pg yr^{-1}) and reaching the minimum in fall (around 0.33 Pg yr^{-1}) in general. Previous studies have also pointed out that dust emissions over different African regions show distinct variations (Bakker et al., 2019; Shao et al., 2010), attributed to differences in geographical properties (Knippertz et al., 2007),

vegetation cover (Mahowald et al., 2006; Kim et al., 2017), and meteorological mechanisms on a local scale (Alizadeh-Choobari et al., 2014; Wang et al., 2017; Roberts and Knippertz, 2012). Consequently, there exists substantial seasonal change in dust source regions. For instance, during boreal winter, the Bodélé Depression in northern Chad is found to be the most active triggered by the Harmattan winds, while the northwestern African dust sources become less active in contrast with the condition in boreal summer (Ben-Ami et al., 2012; Prospero et al., 2014). Therefore, we further analyze the emission variability over five different source regions in northern Africa (Figure 1 and Table S1). On an annual basis, the contribution to total northern African dust emission is the largest from Region A (west Sahara, 36% ± 4.0%), followed by Region D (central Sahel including the Bodélé Depression, 21% ± 4.7%), Region B (central Sahara, 13% ± 2.6%), Region C (east Sahara, 12% ± 1.0%), and Region E (west Sahel, 6.5% ± 0.64%). The emission fluxes, however, are the most intensive in Region D, up to 11 ± 2.1 g month^{-1} m^{-2} and are generally below 5 g month^{-1} m^{-2} over the other regions.

Concerning the seasonality, higher dust emission tends to occur in boreal spring and winter, with the largest emission flux of 19 ± 4.7 g month^{-1} m^{-2} from Region D. As shown in Figure 6 and S1, the emissions peak in boreal spring for Region A, B and C, but in winter for Region D and E. There is also a secondary peak in summer emissions for Region E. Correlation analysis between dust emissions and meteorological variables suggests that the seasonality is mainly driven by high surface wind speeds (with r of 0.79-0.96 and 0.68-0.97 for the 75th and 95th percentiles of 10-m wind speeds, respectively). Apparent negative correlation is also found between precipitation (soil moisture, Figure S1) and dust emission in Region D with r of -0.69 (-0.67).

Similar seasonality is also reported by Cowie et al. (2014), who suggested that the strongest dust season in winter in central Sahel is driven by strong harmattan winds and frequent Low level Jet breakdown, and the second peak in summer in west Sahel could be explained by the summer monsoon combined with the Sahara Heat Low. The

study also suggested the dominance of strong wind frequency in the seasonal variation of the emission frequencies. Fiedler et al. (2013) also found a maximum of emission flux over the Bodélé Depression in winter and the highest emission flux in spring in west Sahara. The study suggested that near-surface peak winds associated with Nocturnal Low-Level Jets is a driver of mineral dust emissions. Negative correlation between dust emissions and soil moisture has also been revealed by Yu et al. (2017) and Pierre et al. (2012), as the decreased vegetation growth in response to dry soil would result in enhanced dust emissions.

It is also worth noting that the interannual variation in dust emission is much larger during the wet season (0.96 ± 0.25 Pg yr^{-1}, Table 3) than on an annual basis (0.73 ± 0.12 Pg yr^{-1}). Moreover, while the annual emissions gradually decrease from 2013 to 2017, the emissions during the wet season peak in 2015. The obviously different behavior between the annual emissions and emissions during the wet season suggests that predictions of future impact of African dust emissions over the Amazon Basin in response to climate change should focus on the wet season rather than the annual average, as the former is more related to the export of African dust towards the Amazon Basin.

4.2 Transatlantic transport of African dust

The amount of African dust reaching the Amazon Basin depends not only on the dust emission fluxes, but also the transport path. Associated with the annual oscillation of ITCZ, the dust column burden shows a steep east-west gradient across the ocean with two major paths for different seasons (Fig. S4): oneoutflow of African dust moves slightly southwest toward South America in boreal winter and spring, and the other moves west towards the Caribbean in boreal summer and fall. (Moran-Zuloaga et al., 2018; Ben-Ami et al., 2012). Therefore, although higher dust load over the coastal region of North Africa is found in summer (> 500 mg m^{-2}), dust reaching the Amazon Basin is less than 10 mg m^{-2}. In contrast, dust load over the Amazon Basin could reach up to 50 mg m^{-2} in spring and winter.

In addition to the transport path, the changes in dust column burden along the transport towards the Amazon Basin isare also sensitive to its removal rate, namely the lifetime against deposition over the Atlantic. Assuming first-order removal of dust

588 aerosols, we further derived seasonal e-folding lifetime (hereinafter referred to as

589 lifetime, τ) of simulated dust during 2013 − 2017, based on the logarithm of the dust

590 column burden against travel time over the AOaTP (~~Fig. 7).~~ Figure 7) using Equation

591 1:

592 $$\tau = \frac{L}{v \times slope} \hspace{3cm} (1)$$

593 where L is the distance of 1-degree longitude averaged over 5° S − 25° N in unit of m

594 degree^{-1}; v is the wind speed in unit of m s^{-1}; and *slope* is the gradient of the linear

595 trend line based on the logarithm of dust burden against the distance in degree

596 between 20 ºW and 50 ºW.

597 Estimated dust lifetime is the shortest (1.4 ± 0.098 d) in winter, followed by fall and

598 spring (1.9 ± 0.33 d and 2.3 ± 0.31 d, respectively), while the lifetime in summer is

599 the longest (4.2 ± 0.68 d). The interannual variability of the lifetime is small in winter

600 with relative standard deviation (RSD) of 7.0%, but relatively large in fall with RSD

601 of 17%.

602 The short lifetime in winter is generally associated with high deposition ~~(with 0.18 ±~~

603 ~~0.034 Pg a^{-1} accounting 20% of the emission of Northern Africa, Table S2).~~flux

604 (including both dry and wet deposition). As shown in ~~Fig.~~Figure 8, the ~~spatial~~

605 ~~distribution of dust deposition is similar to that of dust burden, again illustrating the~~

606 ~~main transport paths. The~~ largest dust deposition flux (> 1000 ng m^{-2} s^{-1}) is found over

607 the source regions in northern Africa, especially in spring and winter, and is mainly

608 due to dry deposition (accounting for more than 80%). As a result, 48% – 64% of total

609 emission in northern Africa is deposited within the source region~~.~~ (Table S2). The

610 deposition flux over the AOaTP, also shows strong seasonality, with a maximum of

611 ~530 ng m^{-2} s^{-1} in winter and a minimum of ~180 ng m^{-2} s^{-1} in fall, and is mainly

612 driven by wet deposition (accounting for 76% on average). ~~Again, although the~~

613 ~~emissions are similar in spring and winter, the deposition flux is much larger in~~

614 ~~winter, consistent with the relatively shorter lifetime in winter discussed above. On~~

615 ~~the other hand, the highest dust burden (144 ± 58 mg m^{-2}) over the AOaTP is found in~~

616 ~~summer mainly associated with its longer lifetime, followed by 127 ± 24, 98 ± 35, and~~

21

57 ± 20 mg m⁻² in winter, spring and fall, respectively. The deposition over the AOaTP only accounts for 7.720% of total emission in northern Africa in Springwinter, in contrast to 207.7% in spring, consistent with the relatively shorter lifetime in winter. discussed above.

5.The seasonality in the deposition fluxes and the consequent dust lifetime depends not only on precipitation but also the vertical pathways of dust transport across the Atlantic. Dust aerosols aloft at higher altitude reach further west and have relatively longer lifetime. Significant differences in dust vertical distributions along the transport pathways have been revealed from the CALIOP measurements, which show that more dust is transported above 2km in summer while the dust layer is the shallowest in winter (Liu et al., 2012).

4.3 The influence of African dust over the Amazon Basin

54.3.1 Surface aerosol concentrations and AOD

Figure 9 shows the time series of observed and simulated aerosol mass concentrations at ATTO in January − June for the period of 2014 − 2016. Observed mean concentration in wet season is 9.3 ± 7.6 μg m⁻³, of which 83% is from coarse aerosol (7.7 μg m⁻³), while simulated concentration is 11 ± 6.7 μg m⁻³, with dust contribution of 65% (7.2 μg m⁻³). The slight model bias could be to some extent explained by the difference in background concentrations (1.9 and 5.1 μg m⁻³ for the observation and model data, respectively). During the wet season, observed coarse aerosol concentrations frequently exceed 9 μg m⁻³, and could be up to 50 μg m⁻³. Most of observed peaks are found in February − March of 2014 and 2016, and in February − April of 2015. The high correlation (r of $0.52 − 0.71$) between observed coarse aerosols and simulated dust concentrations suggests that observed strong variation in coarse aerosols is mainly driven by the influence of dust. Rizzolo et al. (2017) conducted aerosol measurements at ATTO from 19 March to 24 April 2015. The study showed the arrival of African dust between 3 and 6 April when the highest concentrations of PM_{10}, soluble Fe (III) and Fe (II) were recorded at ATTO. The peak value of 23 μg m⁻³ for PM_{10} was observed on 5 April. This dust event is well reproduced in this study with the peak value of 28 μg m⁻³ for PM_{10} on the same day and the dust contribution to PM_{10} reaching above 70%. The co-occurrence of elevated sea salt concentration (reaching 2.5 μg m⁻³) during this event is also found in this study, consistent with previous studies which show mixed transport

649 of African dust and marine aerosol to the basin (Wang et al., 2016; Ben-Ami et al., 2010; Rizzolo et al., 2017; Adachi et al., 2020).

651 The dust peaks are generally associated with large dust emission and/or efficient trans-Atlantic transport (e.g. relatively longer lifetime). For example, the relatively higher dust concentrations in the wet season of 2015 (except for February) are generally associated with higher emissions (1.2 − 1.5 Pg ~~a~~yr^{-1}) compared with the year of 2014 and 2016 (0.68 – 1.0 Pg ~~a~~yr^{-1}, see Table S3). On the other hand, although emissions in February 2016 (0.95 Pg ~~a~~yr^{-1}) is slightly lower than those in February 2014 (1.2 Pg ~~a~~yr^{-1}), the relatively longer lifetime (1.7 d vs. 1.5 d) may help explain the high dust concentrations during that period. It should be noted that the lifetime estimated here represents the export efficiency averaged over a relatively large domain and a long-time scale (e.g. one month). Besides, the influence of African dust on the ATTO site is also subject to the variations of transport paths and precipitation fields.

663 Over the whole Amazon Basin, simulated ~~average~~mean surface dust concentrations in the wet season of 2013 − 2017 are 5.7 ± 1.3 µg m^{-3}, with ~~maxima over 15~~a maximum of 7.9 µg m^{-3} in 2015 driven mainly by the relatively high dust emission flux. The maxima of surface dust concentrations are found in the northeast corner of rainforest ~~and a~~(over 15 µg m^{-3}) with a clearly decreasing trend towards southwestern direction (~~Fig.~~Figure 10). The dust contribution to surface aerosol concentrations ~~is 47% ± 5.0% (up to 70% in the north corner).~~averaged over the whole basin is 40% ± 4.5%, again with the maximum of 48% found in 2015. The location with the largest dust contributions (up to 70% in the north corner) slightly shifted inland compared to the spatial distribution of dust concentration. This could be explained by relatively higher influence of sea salt aerosols along the coast. ~~The ATTO site has dust concentrations (around 8.1 ±1.8 µg m^{-3} (accounting for 63% ± 7.9% of total aerosol concentrations on average) in wet season, and thus could be representative of the whole Amazon Basin. Based on single-particle analysis using a quantitative energy-dispersive electron probe X-ray microanalysis, Wu et al. (2019) found that aged mineral dust and sea salts account for 37 % 70 % of the super-micron aerosol at ATTO site during the~~

23

679 ~~wet season, consistent with our result. The contribution~~30-50% near the coast of ~~DOD~~

680 ~~to AOD at 675 nm over most areas of the Amazon Basin (Fig. 11) is in~~South

681 America). Although the ~~range of 10 − 50% (26% ± 4.7% on average) during the wet~~

682 ~~season of 2013 − 2017, with maxima in the northern Amazon Basin. The~~ emission

683 fluxes of both sea salt and dust ~~contribution to total AOD is relatively smaller than~~

684 ~~that to surface aerosol concentrations, mainly because of the relatively lower MEE~~are

685 largely determined by surface winds, the interannual variability of dust ~~aerosols~~

686 ~~compared to other aerosols.~~

687 ~~**5.2 Frequency of dust events**~~concentrations is larger than sea salt over the Amazon

688 Basin (20% vs. 10%) as the former is also sensitive to the export efficiency across the

689 Atlantic Ocean as discussed above.

690 Figure 10c also shows the frequency of dust events over the Amazon Basin, estimated

691 as the number of days when daily surface dust concentrations ~~reach~~reaching the

692 threshold of 9 µg m^{-3} ~~on daily basis as defined in~~ (Moran-Zuloaga et al.~~. (~~., 2018)

693 ~~over~~divided by the ~~Amazon Basin~~total number of days in the wet season of 2013 −

694 2017. Dust frequency averaged over the whole region is around 18% ± 4.6% and

695 decreases from 50 − 60% at the northeast coast to < 1% in southern inland. The

696 frequency of dust events at ATTO site is around 32%, close to the median of the

697 range. The interannual variation of the frequency~~,~~ (represented by RSD), however, has

698 an opposite trend,~~ with RSD~~ gradually increasing from 10% at the northeast coast to

699 over 100% in southern inland (36% at ATTO). During dust events, the dust mass

700 concentration ~~of~~at ATTO reaches 16 ± 2.9 µg m^{-3} (three times as high as that over the

701 whole wet season), accounting for around ~~77~~75% ± 5.~~8~~3% of total aerosol~~.~~ (Figure

702 10d). Similarly, under the influence of the long-range transport of Saharan dust

703 plumes, Moran-Zuloaga et al. (2018) observed mass concentrations 14 ± 12 µg m^{-3} for

704 coarse aerosol at the same site, accounting for 93% of total observed aerosol.

705

706 **4.3.2 AOD**

707 The contribution of DOD to AOD at 550 nm over most areas of the Amazon Basin

(Figure 11) is in the range of 10 − 50% (23% ± 4.4% on average) during the wet

season of 2013 − 2017, with maxima in the northern Amazon Basin. The dust

contribution to total AOD is relatively smaller than that to surface aerosol

concentrations, mainly because of the relatively lower MEE of dust aerosols

compared to other aerosols. There also ~~exits~~exists large difference in DOD between

the whole wet season and dust events: 0.~~019~~021 ± 0.~~0047~~0055 vs. 0.~~038~~055 ± 0.~~0074~~

~~(at wavelength of 675 nm)~~0076 averaged over the Amazon Basin. A maximum of 0.31

on a daily basis is found on 1 Mar 2016 at the northeast corner (55° W, 4° N) of the

Amazon Basin during the study period. During dust events, dust aerosols dominate

AOD (~~50~~40% − 60%) over most regions of the Amazon Basin. At ATTO site, DOD is

0.~~029~~034 ± 0.~~0076~~0088 and 0.~~054~~063 ± 0.~~0074~~0087, accounting for ~~41~~37% and

~~57~~53% of AOD over the whole wet season and dust events, respectively. The largest

dust contribution (up to ~~84~~81%) with DOD of 0.~~15~~18 at ATTO site is found on 24 Jan

2015. Consistent with our results, previous studies by Baars et al. (2011) and Baars et

al. (2012) reported DOD (532 nm) of up to 0.18 and AOD of ~0.14 when affected by

strong influence of Saharan dust at a similar Amazon site (60° 2.3′ W, 2° 35.9′ S).

~~5~~4.~~3~~.3 Dust deposition and related nutrient input

The spatial distribution of dust deposition over the Amazon Basin is also shown in

~~Fig.~~Figure 8. The mean dust deposition flux in wet season is 2.0 ± 0.35 g m^{-2} ~~a~~yr^{-1},

much higher than in dry seasons (August to November, 0.35 ± 0.16 g m^{-2} ~~a~~yr^{-1}). The

maximum (2.6 g m^{-2} ~~a~~yr^{-1}) is found in the year 2015 due to relatively large dust

emission and efficient trans-Atlantic transport. With emission of 0.96 ± 0.25 Pg ~~a~~yr^{-1}

in wet season (0.73 ± 0.12 Pg ~~a~~yr^{-1} on annual average), only 1.9% (1.4%) of African

dust is deposited into the Amazon Basin (dominated by wet deposition) while

relatively large part is deposited over the AOaTP (13% in the wet season and 14% on

annual average) and northern Africa (49% in the wet season).

Assuming mass fractions of 4.4%, 0.082%, and 1.8% for iron, phosphorus, and

magnesium respectively in the African dust (Bristow et al., 2010; Chiemeka et al.,

2007), we derive deposition fluxes of 88 ± 15 mg m^{-2} yr^{-1}, 1.6 ± 0.29 mg m^{-2} yr^{-1} and 36 ± 6.3 mg m^{-2} yr^{-1} for iron, phosphorus and magnesium respectively into the Amazon rainforest during the wet season and 52 ± 8.7, 0.97 ± 0.16 and 21 ± 3.6 mg m^{-2} yr^{-1} on annual average (Figure 12). It should be noted that there exits large spatial variation of nutrient input into the Amazon Basin associated with the patterns of dust burden and dust deposition flux. The deposition flux decreases from over 70 mg m^{-2} yr^{-1} at northeast coast to less than 7 mg m^{-2} yr^{-1} in inland for magnesium and decreases from > 9 mg m^{-2} yr^{-1} at northeast coast to less than 1 mg m^{-2} yr^{-1} in southwestern Basin for phosphorus during the wet season. Similarly, the deposition flux of iron during the wet season decreases from over 500 mg m^{-2} yr^{-1} at northeast coast to less than 15 mg m^{-2} yr^{-1} in the southwest and is above 50 mg m^{-2} yr^{-1} in most of the Amazon Basin. It seems that the nutrient input from Africa dust may play a significant role in the northeastern part of the Amazon Basin, not in the southwest. Table 4 summarized the estimates of dust and associated phosphorus deposition into the Amazon Basin from previous studies. The estimated fluxes of dust and associated phosphorus deposition are in the range of $0.81 - 19$ g m^{-2} yr^{-1} and $0.48 - 16$ mg m^{-2} yr^{-1}. The large range is mainly driven by the high values (19 g m^{-2} yr^{-1} and 16 mg m^{-2} yr^{-1} for dust and associated phosphorus, respectively) from the study of Swap et al. (1992). Based on observations during storm events and dust climatology, the study estimated dust importation into the northeastern basin, which is most subject to the intrusion of African dust. Besides the discrepancy in defined regions, the wide range could also be partly explained by the application of different methods and associated intrinsic uncertainties as mentioned in the Introduction. For instance, the estimates from Swap et al. (1992) are mainly based on 1-month field measurements at three sites located in the northeastern basin. Assumption about air exchange rate across the coast to the basin, duration of dust storms as well as dust concentrations contained in the dust plumes had to been made to extrapolate the dust deposition into the Amazon Basin. Similarly, bias could also arise from insufficient observations available to constrain models or satellite retrievals. Additional uncertainty may also stem from the

assumption about the P mass fraction, ranging from 0.07% to 0.108%. Our results are similar to the finding of Prospero et al. (2020), which has also been constrained by the observation at Cayenne.

According to Salati and Vose (1984), the total amount of phosphorous and magnesium is 21.6 g m^{-2} and 29.8 g m^{-2}, respectively, in the ecosystem of the Amazon Basin (14.7 and 2.3 g m^{-2} respectively in the soil). On the other hand, Vitousek and ~~R L~~ Sanford (1986) reported a loss of $0.8 - 4$ mg m^{-2} ~~a~~yr^{-1} for phosphorus and 810 mg m^{-2} ~~a~~yr^{-1} for magnesium in Brazilian ecosystem to surface waters. Estimated nutrient input from African dust in our study accounts for 0.011% and 1.6% of total phosphorous and magnesium in the soil over the Amazon Basin during the wet season (0.0066% and 0.91% on annual average), and could almost compensate the hydrologic losses of phosphorous in Brazilian forest ecosystem. Similarly, Abouchami et al. (2013) pointed out that most of the Amazonian rainforest is a system with an internal recycling of nutrients. But the extra influx of nutrients from African dust might account for a significant portion of the net ouflux, i.e. dissolved discharge of nutrients into rivers. Keep in mind that the estimates of nutrients influx are subject to the uncertainties in the estimates of dust flux as well as the mass fractions of nutrients containted in the dust. In addition, marine aerosols and biomassburning aerosols mixed with the LRT of African dust may also play a role for certain essential nutrients (Prospero et al., 2020; Abouchami et al., 2013). More observations including the mass fraction of nutrient in dust aerosols and the deposition fluxes of those elements in the Amazon Basin are necessarily required in the future work to better evaluate the nutrient input associated with the African dust intrusion.

5 ~~6.~~ **Conclusion**

In this study, we use the GEOS-Chem model with optimized particle mass size distribution (PMSD) of dust aerosols to investigate the influence of the export of African dust towards the Amazon Basin during $2013 - 2017$. The model performance is constrained by multiple datasets obtained from AERONET, MODIS, as well as

Cayenne and ATTO sites in the Amazon Basin~~, including particle size distribution over Africa, aerosol optical depth (AOD) over Africa and the Atlantic Ocean as well as coarse and total aerosols concentrations in the Amazon Basin.~~

~~Simulated dust emission from northern Africa is 0.73 ± 0.12 Pg a^{-1}, accounting for more than 70% of global dust emission. There exists a strong seasonality in dust emission with peaks in spring or winter, which varies with source regions and is mainly driven by high surface wind speeds. It is worth noting that no consistent decline is found for dust emission during the wet season, when the export of African dust towards the Amazon Basin is more efficient driven by the southward movement of ITCZ.~~

~~In addition to the transport path associated with the oscillation of ITCZ, the export efficiency of African dust towards the Amazon basin is sensitive to the removal of dust aerosol along the trans-Atlantic transport, which also depends on assumed PMSD of dust aerosols in the model..~~ The optimized PMSD in this study well captures observed AOD regarding both the mean value as well as the decline rate of the logarithm of AOD over the Atlantic Ocean along the transport path (AOaTP), while the other two PMSD schemes tend to overestimate the decline rate by 11% and underestimate the mean value by up to ~40%.

Simulated dust emission from northern Africa is 0.73 ± 0.12 Pg yr^{-1}, accounting for more than 70% of global dust emission. There exists a strong seasonality in dust emission with peaks in spring or winter, which varies with source regions. The correlation analysis suggests high surface wind speeds and low soil moisture as a major driver for dust emissions. In addition to the transport path associated with the oscillation of ITCZ, the export efficiency of African dust towards the Amazon basin is sensitive to the removal of dust aerosol along the trans-Atlantic transport, which depends on both assumed PMSD of dust aerosols in the model and meteorological fields (i.e. precipitation and vertical transport path). The study further estimates the e-folding lifetime of dust aerosols along the trans-Atlantic transport based on the logarithm of the dust column burden against travel time over the AOaTP. The shortest

lifetime (1.4 d) is found for winter associated with high deposition flux, while the

highest dust burden over the AOaTP is found in summer mainly associated with its

longer lifetime (4.2 d).

Simulated surface dust concentration averaged over the whole Amazon Basin is 5.7 ±

1.3 µg m^{-3} during the wet season of 2013 – 2017, contributing ~~47% ±~~ 40% ± 4.~~5.0~~%

to total surface aerosols. Observed dust peaks at the ATTO site are generally

associated with large dust emission and/or efficient trans-Atlantic transport. The

frequency of dust events is 18% ± 4.6% averaged over the Amazon Basin and up to

50% − 60% at the northeast coast. During the dust events, DOD is around 0.~~038~~055±

0.0076 and dominate total AOD over most of the Amazon Basin. Associated with the

deposition of African dust, the study estimated annual inputs of 52 ± 8.7, 0.97 ± 0.16

and 21 ± 3.6 mg m^{-2} ~~a~~yr^{-1} for iron, phosphorus and magnesium into the Amazon

rainforest, which may well compensate the hydrologic losses of nutrients in the forest

ecosystem.

865

866   Competing interests.

867   Hang Su and Yafang Cheng are members of the editorial board of Atmospheric Chemistry and

868   Physics.

869

870   Data availability.

871   OPS data used in this study could be found at https://www.attodata.org/. Other datasets are

872   available upon request.

873

874 References

875   Abouchami, W., Näthe, K., Kumar, A., Galer, S. J. G., Jochum, K. P., Williams, E., Horbe, A.

876   M. C., Rosa, J. W. C., Balsam, W., Adams, D., Mezger, K., and Andreae, M. O.:

877   Geochemical and isotopic characterization of the Bodélé Depression dust source and

878   implications for transatlantic dust transport to the Amazon Basin, Earth Planet. Sc. Lett.,

879   380, 112-123, https://doi.org/10.1016/j.epsl.2013.08.028, 2013.

880   Adachi, K., Oshima, N., Gong, Z., de Sá, S., Bateman, A. P., Martin, S. T., de Brito, J. F.,

881   Artaxo, P., Cirino, G. G., Sedlacek Iii, A. J., and Buseck, P. R.: Mixing states of Amazon

882   basin aerosol particles transported over long distances using transmission electron

883   microscopy, Atmos. Chem. Phys., 20, 11923-11939, 10.5194/acp-20-11923-2020, 2020.

884   Alizadeh-Choobari, O., Sturman, A., and Zawar-Reza, P.: A global satellite view of the

885   seasonal distribution of mineral dust and its correlation with atmospheric circulation,

886   Dynam. Atmos. Oceans, 68, 20-34, https://doi.org/10.1016/j.dynatmoce.2014.07.002,
887   2014.

888 Andreae, M. O., Berresheim, H., Bingemer, H., Jacob, D. J., Lewis, B. L., Li, S.-M., and
889   Talbot, R. W.: The atmospheric sulfur cycle over the Amazon Basin: 2. Wet season, J.
890   Geophys. Res., 95, 16813-16824, https://doi.org/10.1029/JD095iD10p16813, 1990.

891 Andreae, M. O., Acevedo, O. C., Araùjo, A., Artaxo, P., Barbosa, C. G. G., Barbosa, H. M. J.,
892   Brito, J., Carbone, S., Chi, X., Cintra, B. B. L., da Silva, N. F., Dias, N. L., Dias-Júnior,
893   C. Q., Ditas, F., Ditz, R., Godoi, A. F. L., Godoi, R. H. M., Heimann, M., Hoffmann, T.,
894   Kesselmeier, J., Könemann, T., Krüger, M. L., Lavric, J. V., Manzi, A. O., Lopes, A. P.,
895   Martins, D. L., Mikhailov, E. F., Moran-Zuloaga, D., Nelson, B. W., Nölscher, A. C.,
896   Santos Nogueira, D., Piedade, M. T. F., Pöhlker, C., Pöschl, U., Quesada, C. A., Rizzo,
897   L. V., Ro, C. U., Ruckteschler, N., Sá, L. D. A., de Oliveira Sá, M., Sales, C. B., dos
898   Santos, R. M. N., Saturno, J., Schöngart, J., Sörgel, M., de Souza, C. M., de Souza, R. A.
899   F., Su, H., Targhetta, N., Tóta, J., Trebs, I., Trumbore, S., van Eijck, A., Walter, D.,
900   Wang, Z., Weber, B., Williams, J., Winderlich, J., Wittmann, F., Wolff, S., and Yáñez-
901   Serrano, A. M.: The Amazon Tall Tower Observatory (ATTO): overview of pilot
902   measurements on ecosystem ecology, meteorology, trace gases, and aerosols, Atmos.
903   Chem. Phys., 15, 10723-10776, 10.5194/acp-15-10723-2015, 2015.

904 Ansmann, A., Baars, H., Tesche, M., Müller, D., Althausen, D., Engelmann, R., Pauliquevis,
905   T., and Artaxo, P.: Dust and smoke transport from Africa to South America: Lidar
906   profiling over Cape Verde and the Amazon rainforest, Geophys. Res. Lett., 36,
907   https://doi.org/10.1029/2009GL037923, 2009.

908 Baars, H., Ansmann, A., Althausen, D., Engelmann, R., Artaxo, P., Pauliquevis, T., and Souza,
909   R.: Further evidence for significant smoke transport from Africa to Amazonia, Geophys.
910   Res. Lett., 38, https://doi.org/10.1029/2011GL049200, 2011.

911 Baars, H., Ansmann, A., Althausen, D., Engelmann, R., Heese, B., Müller, D., Artaxo, P.,
912   Paixao, M., Pauliquevis, T., and Souza, R.: Aerosol profiling with lidar in the Amazon
913   Basin during the wet and dry season, J. Geophys. Res., 117,
914   https://doi.org/10.1029/2012JD018338, 2012.

915 Bakker, N. L., Drake, N. A., and Bristow, C. S.: Evaluating the relative importance of
916   northern African mineral dust sources using remote sensing, Atmos. Chem. Phys., 19,
917   10525-10535, 10.5194/acp-19-10525-2019, 2019.

918 Barkley, A. E., Prospero, J. M., Mahowald, N., Hamilton, D. S., Popendorf, K. J., Oehlert, A.
919   M., Pourmand, A., Gatineau, A., Panechou-Pulcherie, K., Blackwelder, P., and Gaston,
920   C. J.: African biomass burning is a substantial source of phosphorus deposition to the
921   Amazon, Tropical Atlantic Ocean, and Southern Ocean, Proceedings of the National
922   Academy of Sciences, 116, 16216-16221, 10.1073/pnas.1906091116, 2019.

923 Ben-Ami, Y., Koren, I., Altaratz, O., Kostinski, A., and Lehahn, Y.: Discernible rhythm in the
924   spatio/temporal distributions of transatlantic dust, Atmos. Chem. Phys., 12, 2253-2262,
925   10.5194/acp-12-2253-2012, 2012.

926 Ben-Ami, Y., Koren, I., Rudich, Y., Artaxo, P., Martin, S. T., and Andreae, M. O.: Transport of
927   North African dust from the Bodélé depression to the Amazon Basin: a case study,
928   Atmos. Chem. Phys., 10, 7533-7544, 10.5194/acp-10-7533-2010, 2010.

929 Bristow, C. S., Hudson-Edwards, K. A., and Chappell, A.: Fertilizing the Amazon and

31

equatorial Atlantic with West African dust, Geophys. Res. Lett., 37,
https://doi.org/10.1029/2010GL043486, 2010.

Chen, Y., Kreidenweis, S. M., McInnes, L. M., Rogers, D. C., and DeMott, P. J.: Single
particle analyses of ice nucleating aerosols in the upper troposphere and lower
stratosphere, Geophys. Res. Lett., 25, 1391-1394, 10.1029/97gl03261, 1998.

Chiemeka, I. U., Oleka, M. O., and Chineke, T.: Determination of aerosol metal composition
and concentration during the 2001/2002 Harmattan season at Uturu, Nigeria, Global J.
Pure Appl. Sci., 13, 10.4314/gjpas.v13i3.16734, 2007.

Cowie, S. M., Knippertz, P., and Marsham, J. H.: A climatology of dust emission events from
northern Africa using long-term surface observations, Atmos. Chem. Phys., 14, 8579-
8597, 10.5194/acp-14-8579-2014, 2014.

Demott, P. J., Sassen, K., Poellot, M. R., Baumgardner, D., Rogers, D. C., Brooks, S. D.,
Prenni, A. J., and Kreidenweis, S. M.: African dust aerosols as atmospheric ice nuclei,
Geophys. Res. Lett., 30, https://doi.org/10.1029/2003GL017410, 2003.

Di Biagio, C., Formenti, P., Balkanski, Y., Caponi, L., Cazaunau, M., Pangui, E., Journet, E.,
Nowak, S., Andreae, M. O., Kandler, K., Saeed, T., Piketh, S., Seibert, D., Williams, E.,
and Doussin, J. F.: Complex refractive indices and single-scattering albedo of global dust
aerosols in the shortwave spectrum and relationship to size and iron content, Atmos.
Chem. Phys., 19, 15503-15531, 10.5194/acp-19-15503-2019, 2019.

Drury, E., Jacob, D. J., Spurr, R. J. D., Wang, J., Shinozuka, Y., Anderson, B. E., Clarke, A.
D., Dibb, J., McNaughton, C., and Weber, R.: Synthesis of satellite (MODIS), aircraft
(ICARTT), and surface (IMPROVE, EPA-AQS, AERONET) aerosol observations over
eastern North America to improve MODIS aerosol retrievals and constrain surface
aerosol concentrations and sources, J. Geophys. Res., 115,
https://doi.org/10.1029/2009JD012629, 2010.

Dubovik, O., Holben, B., Eck, T. F., Smirnov, A., Kaufman, Y. J., King, M. D., Tanré, D., and
Slutsker, I.: Variability of Absorption and Optical Properties of Key Aerosol Types
Observed in Worldwide Locations, J. Atmos. Sci., 59, 590-608,
http://doi.org/10.1175/1520-0469(2002)059<0590:VOAAOP>2.0.CO;2, 2002.

Duncan Fairlie, T., Jacob, D. J., and Park, R. J.: The impact of transpacific transport of
mineral dust in the United States, Atmos. Environ., 41, 1251-1266,
https://doi.org/10.1016/j.atmosenv.2006.09.048, 2007.

Dusek, U., Frank, G. P., Hildebrandt, L., Curtius, J., Schneider, J., Walter, S., Chand, D.,
Drewnick, F., Hings, S., Jung, D., Borrmann, S., and Andreae, M. O.: Size Matters More
Than Chemistry for Cloud-Nucleating Ability of Aerosol Particles, Science, 312, 1375-
1378, doi:10.1126/science.1125261, 2006.

Enfield, D. B., Mestas-Nuñez, A. M., and Trimble, P. J.: The Atlantic Multidecadal
Oscillation and its relation to rainfall and river flows in the continental U.S, Geophys.
Res. Lett., 28, 2077-2080, https://doi.org/10.1029/2000GL012745, 2001.

Evan, A. T., Flamant, C., Gaetani, M., and Guichard, F.: The past, present and future of
African dust, Nature, 531, 493-495, 10.1038/nature17149, 2016.

Formenti, P., Andreae, M. O., Lange, L., Roberts, G., Cafmeyer, J., Rajta, I., Maenhaut, W.,
Holben, B. N., Artaxo, P., and Lelieveld, J.: Saharan dust in Brazil and Suriname during
the Large-Scale Biosphere-Atmosphere Experiment in Amazonia (LBA) - Cooperative

LBA Regional Experiment (CLAIRE) in March 1998, J. Geophys. Res., 106, 14919-14934, 10.1029/2000JD900827, 2001.

Gläser, G., Wernli, H., Kerkweg, A., and Teubler, F.: The transatlantic dust transport from North Africa to the Americas—Its characteristics and source regions, Journal of Geophysical Research: Atmospheres, 120, 11,231-211,252, https://doi.org/10.1002/2015JD023792, 2015.

Herbert, R. J., Krom, M. D., Carslaw, K. S., Stockdale, A., Mortimer, R. J. G., Benning, L. G., Pringle, K., and Browse, J.: The Effect of Atmospheric Acid Processing on the Global Deposition of Bioavailable Phosphorus From Dust, Global Biogeochemical Cycles, 32, 1367-1385, https://doi.org/10.1029/2018GB005880, 2018.

Highwood, E. J., Haywood, J. M., Silverstone, M. D., Newman, S. M., and Taylor, J. P.: Radiative properties and direct effect of Saharan dust measured by the C-130 aircraft during Saharan Dust Experiment (SHADE): 2. Terrestrial spectrum, J. Geophys. Res., 108, https://doi.org/10.1029/2002JD002552, 2003.

Holanda, B. A., Pöhlker, M. L., Walter, D., Saturno, J., Sörgel, M., Ditas, J., Ditas, F., Schulz, C., Franco, M. A., Wang, Q., Donth, T., Artaxo, P., Barbosa, H. M. J., Borrmann, S., Braga, R., Brito, J., Cheng, Y., Dollner, M., Kaiser, J. W., Klimach, T., Knote, C., Krüger, O. O., Fütterer, D., Lavrič, J. V., Ma, N., Machado, L. A. T., Ming, J., Morais, F. G., Paulsen, H., Sauer, D., Schlager, H., Schneider, J., Su, H., Weinzierl, B., Walser, A., Wendisch, M., Ziereis, H., Zöger, M., Pöschl, U., Andreae, M. O., and Pöhlker, C.: Influx of African biomass burning aerosol during the Amazonian dry season through layered transatlantic transport of black carbon-rich smoke, Atmos. Chem. Phys., 20, 4757-4785, 10.5194/acp-20-4757-2020, 2020.

Huneeus, N., Schulz, M., Balkanski, Y., Griesfeller, J., Prospero, J., Kinne, S., Bauer, S., Boucher, O., Chin, M., Dentener, F., Diehl, T., Easter, R., Fillmore, D., Ghan, S., Ginoux, P., Grini, A., Horowitz, L., Koch, D., Krol, M. C., Landing, W., Liu, X., Mahowald, N., Miller, R., Morcrette, J. J., Myhre, G., Penner, J., Perlwitz, J., Stier, P., Takemura, T., and Zender, C. S.: Global dust model intercomparison in AeroCom phase I, Atmos. Chem. Phys., 11, 7781-7816, 10.5194/acp-11-7781-2011, 2011.

Jaeglé, L., Quinn, P. K., Bates, T. S., Alexander, B., and Lin, J. T.: Global distribution of sea salt aerosols: new constraints from in situ and remote sensing observations, Atmos. Chem. Phys., 11, 3137-3157, 10.5194/acp-11-3137-2011, 2011.

Jimenez, J. L., Canagaratna, M. R., Donahue, N. M., Prevot, A. S. H., Zhang, Q., Kroll, J. H., DeCarlo, P. F., Allan, J. D., Coe, H., Ng, N. L., Aiken, A. C., Docherty, K. S., Ulbrich, I. M., Grieshop, A. P., Robinson, A. L., Duplissy, J., Smith, J. D., Wilson, K. R., Lanz, V. A., Hueglin, C., Sun, Y. L., Tian, J., Laaksonen, A., Raatikainen, T., Rautiainen, J., Vaattovaara, P., Ehn, M., Kulmala, M., Tomlinson, J. M., Collins, D. R., Cubison, M. J., Dunlea, J., Huffman, J. A., Onasch, T. B., Alfarra, M. R., Williams, P. I., Bower, K., Kondo, Y., Schneider, J., Drewnick, F., Borrmann, S., Weimer, S., Demerjian, K., Salcedo, D., Cottrell, L., Griffin, R., Takami, A., Miyoshi, T., Hatakeyama, S., Shimono, A., Sun, J. Y., Zhang, Y. M., Dzepina, K., Kimmel, J. R., Sueper, D., Jayne, J. T., Herndon, S. C., Trimborn, A. M., Williams, L. R., Wood, E. C., Middlebrook, A. M., Kolb, C. E., Baltensperger, U., and Worsnop, D. R.: Evolution of Organic Aerosols in the Atmosphere, Science, 326, 5959, 1525-1529, doi:10.1126/science.1180353, 2009.

1018 Kaufman, Y. J.: Dust transport and deposition observed from the Terra-Moderate Resolution
1019   Imaging Spectroradiometer (MODIS) spacecraft over the Atlantic Ocean, Journal of
1020   Geophysical Research, 110, 10.1029/2003jd004436, 2005

1021 Kim, D., Chin, M., Remer, L. A., Diehl, T., Bian, H., Yu, H., Brown, M. E., and Stockwell, W.
1022   R.: Role of surface wind and vegetation cover in multi-decadal variations of dust
1023   emission in the Sahara and Sahel, Atmos. Environ., 148, 282-296,
1024   https://doi.org/10.1016/j.atmosenv.2016.10.051, 2017.

1025 Kim, D., Chin, M., Yu, H., Diehl, T., Tan, Q., Kahn, R. A., Tsigaridis, K., Bauer, S. E.,
1026   Takemura, T., Pozzoli, L., Bellouin, N., Schulz, M., Peyridieu, S., Chédin, A., and Koffi,
1027   B.: Sources, sinks, and transatlantic transport of North African dust aerosol: A
1028   multimodel analysis and comparison with remote sensing data, J. Geophys. Res., 119,
1029   6259-6277, https://doi.org/10.1002/2013JD021099, 2014.

1030 Knippertz, P., Deutscher, C., Kandler, K., Müller, T., Schulz, O., and Schütz, L.: Dust
1031   mobilization due to density currents in the Atlas region: Observations from the Saharan
1032   Mineral Dust Experiment 2006 field campaign, J. Geophys. Res., 112,
1033   https://doi.org/10.1029/2007JD008774, 2007.

1034 Koepke, P., Hess, M., Schult, I., and Shettle, E. P.: Global aerosol data set, Max-Planck
1035   Institute for Meteorology, 44, 1997.

1036 Kok, J. F.: A scaling theory for the size distribution of emitted dust aerosols suggests climate
1037   models underestimate the size of the global dust cycle, Proc Natl Acad Sci U S A, 108,
1038   1016-1021, 10.1073/pnas.1014798108, 2011.

1039 Kok, J. F., Adebiyi, A. A., Albani, S., Balkanski, Y., Checa-Garcia, R., Chin, M., Colarco, P.
1040   R., Hamilton, D. S., Huang, Y., Ito, A., Klose, M., Li, L., Mahowald, N. M., Miller, R.
1041   L., Obiso, V., Pérez García-Pando, C., Rocha-Lima, A., and Wan, J. S.: Contribution of
1042   the world's main dust source regions to the global cycle of desert dust, Atmos. Chem.
1043   Phys., 21, 8169-8193, 10.5194/acp-21-8169-2021, 2021.

1044 Li, Y., Randerson, J. T., Mahowald, N. M., and Lawrence, P. J.: Deforestation Strengthens
1045   Atmospheric Transport of Mineral Dust and Phosphorus from North Africa to the
1046   Amazon, Journal of Climate, 34, 6087-6096, 10.1175/jcli-d-20-0786.1, 2021.

1047 Liu, D., Taylor, J. W., Crosier, J., Marsden, N., Bower, K. N., Lloyd, G., Ryder, C. L., Brooke,
1048   J. K., Cotton, R., Marenco, F., Blyth, A., Cui, Z., Estelles, V., Gallagher, M., Coe, H., and
1049   Choularton, T. W.: Aircraft and ground measurements of dust aerosols over the west
1050   African coast in summer 2015 during ICE-D and AER-D, Atmos. Chem. Phys., 18,
1051   3817-3838, 10.5194/acp-18-3817-2018, 2018.

1052 Liu, H., Jacob, D. J., Bey, I., and Yantosca, R. M.: Constraints from 210Pb and 7Be on wet
1053   deposition and transport in a global three-dimensional chemical tracer model driven by
1054   assimilated meteorological fields, J. Geophys. Res., 106, 12109-12128,
1055   https://doi.org/10.1029/2000JD900839, 2001.

1056 Lucchesi, R.: File Specification for GEOS-5 FP, GMAO Office Note No.4 (Version 1.0), 63
1057   pp., available at: http://gmao.gsfc.nasa.gov/pubs/office_notes, 2013.

1058 Mahowald, N., Albani, S., Engelstaedter, S., Winckler, G., and Goman, M.: Model insight into
1059   glacial–interglacial paleodust records, Quaternary Sci. Rev., 30, 832-854,
1060   https://doi.org/10.1016/j.quascirev.2010.09.007, 2011a.

1061 Mahowald, N., Albani, S., Kok, J. F., Engelstaeder, S., Scanza, R., Ward, D. S., and Flanner,

M. G.: The size distribution of desert dust aerosols and its impact on the Earth system, Aeolian Res., 15, 53-71, https://doi.org/10.1016/j.aeolia.2013.09.002, 2014.

Mahowald, N. M., Artaxo, P., Baker, A. R., Jickells, T. D., Okin, G. S., Randerson, J. T., and Townsend, A. R.: Impacts of biomass burning emissions and land use change on Amazonian atmospheric phosphorus cycling and deposition, Global Biogeochemical Cycles, 19, https://doi.org/10.1029/2005GB002541, 2005.

Mahowald, N., Ward, D. S., Kloster, S., Flanner, M. G., Heald, C. L., Heavens, N. G., Hess, P. G., Lamarque, J.-F., and Chuang, P. Y.: Aerosol Impacts on Climate and Biogeochemistry, Annu. Rev. Env. Resour., 36, 45-74, 10.1146/annurev-environ-042009-094507, 2011b.

Mahowald, N. M. and Kiehl, L. M.: Mineral aerosol and cloud interactions, Geophys. Res. Lett., 30, https://doi.org/10.1029/2002GL016762, 2003.

Mahowald, N. M., Muhs, D. R., Levis, S., Rasch, P. J., Yoshioka, M., Zender, C. S., and Luo, C.: Change in atmospheric mineral aerosols in response to climate: Last glacial period, preindustrial, modern, and doubled carbon dioxide climates, J. Geophys. Res., 111, https://doi.org/10.1029/2005JD006653, 2006.

Martin, R. V., Jacob, D. J., Yantosca, R. M., Chin, M., and Ginoux, P.: Global and regional decreases in tropospheric oxidants from photochemical effects of aerosols, J. Geophys. Res. , 108, https://doi.org/10.1029/2002JD002622, 2003.

Martin, S. T., Andreae, M. O., Artaxo, P., Baumgardner, D., Chen, Q., Goldstein, A. H., Guenther, A., Heald, C. L., Mayol-Bracero, O. L., McMurry, P. H., Pauliquevis, T., Pöschl, U., Prather, K. A., Roberts, G. C., Saleska, S. R., Silva Dias, M. A., Spracklen, D. V., Swietlicki, E., and Trebs, I.: Sources and properties of Amazonian aerosol particles, Rev. Geophys., 48, https://doi.org/10.1029/2008RG000280, 2010a.

Martin, S. T., Andreae, M. O., Althausen, D., Artaxo, P., Baars, H., Borrmann, S., Chen, Q., Farmer, D. K., Guenther, A., Gunthe, S. S., Jimenez, J. L., Karl, T., Longo, K., Manzi, A., Müller, T., Pauliquevis, T., Petters, M. D., Prenni, A. J., Pöschl, U., Rizzo, L. V., Schneider, J., Smith, J. N., Swietlicki, E., Tota, J., Wang, J., Wiedensohler, A., and Zorn, S. R.: An overview of the Amazonian Aerosol Characterization Experiment 2008 (AMAZE-08), Atmos. Chem. Phys., 10, 11415-11438, 10.5194/acp-10-11415-2010, 2010b.

Middleton, N.: Variability and Trends in Dust Storm Frequency on Decadal Timescales: Climatic Drivers and Human Impacts, Geosciences, 9, 261, http://doi.org/10.3390/geosciences9060261, 2019.

Moran-Zuloaga, D., Ditas, F., Walter, D., Saturno, J., Brito, J., Carbone, S., Chi, X., Hrabě de Angelis, I., Baars, H., Godoi, R. H. M., Heese, B., Holanda, B. A., Lavrič, J. V., Martin, S. T., Ming, J., Pöhlker, M. L., Ruckteschler, N., Su, H., Wang, Y., Wang, Q., Wang, Z., Weber, B., Wolff, S., Artaxo, P., Pöschl, U., Andreae, M. O., and Pöhlker, C.: Long-term study on coarse mode aerosols in the Amazon rain forest with the frequent intrusion of Saharan dust plumes, Atmos. Chem. Phys., 18, 10055-10088, 10.5194/acp-18-10055-2018, 2018.

Niedermeier, N., Held, A., Müller, T., Heinold, B., Schepanski, K., Tegen, I., Kandler, K., Ebert, M., Weinbruch, S., Read, K., Lee, J., Fomba, K. W., Müller, K., Herrmann, H., and Wiedensohler, A.: Mass deposition fluxes of Saharan mineral dust to the tropical

northeast Atlantic Ocean: an intercomparison of methods, Atmos. Chem. Phys., 14, 2245-2266, 10.5194/acp-14-2245-2014, 2014.

Pöhlker, C., Walter, D., Paulsen, H., Könemann, T., Rodríguez-Caballero, E., Moran-Zuloaga, D., Brito, J., Carbone, S., Degrendele, C., Després, V. R., Ditas, F., Holanda, B. A., Kaiser, J. W., Lammel, G., Lavrič, J. V., Ming, J., Pickersgill, D., Pöhlker, M. L., Praß, M., Löbs, N., Saturno, J., Sörgel, M., Wang, Q., Weber, B., Wolff, S., Artaxo, P., Pöschl, U., and Andreae, M. O.: Land cover and its transformation in the backward trajectory footprint region of the Amazon Tall Tower Observatory, Atmos. Chem. Phys., 19, 8425-8470, 10.5194/acp-19-8425-2019, 2019.

Pöhlker, M. L., Ditas, F., Saturno, J., Klimach, T., Hrabě de Angelis, I., Araùjo, A. C., Brito, J., Carbone, S., Cheng, Y., Chi, X., Ditz, R., Gunthe, S. S., Holanda, B. A., Kandler, K., Kesselmeier, J., Könemann, T., Krüger, O. O., Lavrič, J. V., Martin, S. T., Mikhailov, E., Moran-Zuloaga, D., Rizzo, L. V., Rose, D., Su, H., Thalman, R., Walter, D., Wang, J., Wolff, S., Barbosa, H. M. J., Artaxo, P., Andreae, M. O., Pöschl, U., and Pöhlker, C.: Long-term observations of cloud condensation nuclei over the Amazon rain forest – Part 2: Variability and characteristics of biomass burning, long-range transport, and pristine rain forest aerosols, Atmos. Chem. Phys., 18, 10289-10331, 10.5194/acp-18-10289-2018, 2018.

Pöschl, U., Martin, S. T., Sinha, B., Chen, Q., Gunthe, S. S., Huffman, J. A., Borrmann, S., Farmer, D. K., Garland, R. M., Helas, G., Jimenez, J. L., King, S. M., Manzi, A., Mikhailov, E., Pauliquevis, T., Petters, M. D., Prenni, A. J., Roldin, P., Rose, D., Schneider, J., Su, H., Zorn, S. R., Artaxo, P., and Andreae, M. O.: Rainforest Aerosols as Biogenic Nuclei of Clouds and Precipitation in the Amazon, Science, 329, 1513-1516, doi:10.1126/science.1191056, 2010.

Prass, M., Andreae, M. O., de Araùjo, A. C., Artaxo, P., Ditas, F., Elbert, W., Förster, J. D., Franco, M. A., Hrabe de Angelis, I., Kesselmeier, J., Klimach, T., Kremper, L. A., Thines, E., Walter, D., Weber, J., Weber, B., Fuchs, B. M., Pöschl, U., and Pöhlker, C.: Bioaerosols in the Amazon rain forest: temporal variations and vertical profiles of Eukarya, Bacteria, and Archaea, Biogeosciences, 18, 4873-4887, 10.5194/bg-18-4873-2021, 2021.

Prospero, J. M., Glaccum, R. A., and Nees, R. T.: Atmospheric transport of soil dust from Africa to South America, Nature, 289, 570-572, 10.1038/289570a0, 1981.

Prospero, J. M., Collard, F.-X., Molinié, J., and Jeannot, A.: Characterizing the annual cycle of African dust transport to the Caribbean Basin and South America and its impact on the environment and air quality, Global Biogeochem. Cy., 28, 757-773, https://doi.org/10.1002/2013GB004802, 2014.

Prospero, J. M., Barkley, A. E., Gaston, C. J., Gatineau, A., Campos y Sansano, A., and Panechou, K.: Characterizing and Quantifying African Dust Transport and Deposition to South America: Implications for the Phosphorus Budget in the Amazon Basin, Global Biogeochem. Cy., 34, e2020GB006536, https://doi.org/10.1029/2020GB006536, 2020.

Ridley, D. A., Heald, C. L., and Ford, B.: North African dust export and deposition: A satellite and model perspective, J. Geophys. Res., 117, https://doi.org/10.1029/2011JD016794, 2012.

Ridley, D. A., Heald, C. L., and Prospero, J. M.: What controls the recent changes in African

mineral dust aerosol across the Atlantic?, Atmos. Chem. Phys., 14, 5735-5747, 10.5194/acp-14-5735-2014, 2014.

Rizzolo, J. A., Barbosa, C. G. G., Borillo, G. C., Godoi, A. F. L., Souza, R. A. F., Andreoli, R. V., Manzi, A. O., Sá, M. O., Alves, E. G., Pöhlker, C., Angelis, I. H., Ditas, F., Saturno, J., Moran-Zuloaga, D., Rizzo, L. V., Rosário, N. E., Pauliquevis, T., Santos, R. M. N., Yamamoto, C. I., Andreae, M. O., Artaxo, P., Taylor, P. E., and Godoi, R. H. M.: Soluble iron nutrients in Saharan dust over the central Amazon rainforest, Atmos. Chem. Phys., 17, 2673-2687, 10.5194/acp-17-2673-2017, 2017.

Roberts, A. and Knippertz, P.: Haboobs: Convectively generated dust storms in West Africa, Weather, 67, 311 - 316, 2012.

Ryder, C. L., Highwood, E. J., Lai, T. M., Sodemann, H., and Marsham, J. H.: Impact of atmospheric transport on the evolution of microphysical and optical properties of Saharan dust, Geophys. Res. Lett., 40, 2433-2438, 10.1002/grl.50482, 2013a.

Ryder, C. L., Highwood, E. J., Rosenberg, P. D., Trembath, J., Brooke, J. K., Bart, M., Dean, A., Crosier, J., Dorsey, J., Brindley, H., Banks, J., Marsham, J. H., McQuaid, J. B., Sodemann, H., and Washington, R.: Optical properties of Saharan dust aerosol and contribution from the coarse mode as measured during the Fennec 2011 aircraft campaign, Atmos. Chem. Phys., 13, 303-325, 10.5194/acp-13-303-2013, 2013b.

Ryder, C. L., Marenco, F., Brooke, J. K., Estelles, V., Cotton, R., Formenti, P., McQuaid, J. B., Price, H. C., Liu, D., Ausset, P., Rosenberg, P. D., Taylor, J. W., Choularton, T., Bower, K., Coe, H., Gallagher, M., Crosier, J., Lloyd, G., Highwood, E. J., and Murray, B. J.: Coarse-mode mineral dust size distributions, composition and optical properties from AER-D aircraft measurements over the tropical eastern Atlantic, Atmos. Chem. Phys., 18, 17225-17257, 10.5194/acp-18-17225-2018, 2018.

Salati, E. and Vose, P. B.: Amazon Basin: A System in Equilibrium, Science, 225, 129-138, doi:10.1126/science.225.4658.129, 1984.

Shao, Y., Fink, A. H., and Klose, M.: Numerical simulation of a continental-scale Saharan dust event, J. Geophys. Res., 115, https://doi.org/10.1029/2009JD012678, 2010.

Shao, Y., Klose, M., and Wyrwoll, K.-H.: Recent global dust trend and connections to climate forcing, J. Geophys. Res., 118, 11,107-111,118, https://doi.org/10.1002/jgrd.50836, 2013.

Sinyuk, A., Torres, O., and Dubovik, O.: Combined use of satellite and surface observations to infer the imaginary part of refractive index of Saharan dust, Geophys. Res. Lett., 30, https://doi.org/10.1029/2002GL016189, 2003.

SWAP, R., GARSTANG, M., GRECO, S., TALBOT, R., and KÅLLBERG, P.: Saharan dust in the Amazon Basin, Tellus B, 44, 133-149, https://doi.org/10.1034/j.1600-0889.1992.t01-1-00005.x, 1992.

Talbot, R. W., Andreae, M. O., Berresheim, H., Artaxo, P., Garstang, M., Harriss, R. C., Beecher, K. M., and Li, S. M.: Aerosol chemistry during the wet season in central Amazonia: The influence of long-range transport, J. Geophys. Res., 95, 16955-16969, https://doi.org/10.1029/JD095iD10p16955, 1990.

van der Does, M., Korte, L. F., Munday, C. I., Brummer, G. J. A., and Stuut, J. B. W.: Particle size traces modern Saharan dust transport and deposition across the equatorial North Atlantic, Atmos. Chem. Phys., 16, 13697-13710, 10.5194/acp-16-13697-2016, 2016.

Vitousek, P. M. and ~~R L~~ Sanford, ~~J.: NUTRIENT CYCLING IN MOIST TROPICAL~~ ~~FOREST~~R. L.: Nutrient Cycling in Moist Tropical Forest, Annual Review of Ecology and Systematics, 17, 137-167, ~~10.1146/annurev.es.17.110186.001033,~~ http://www.jstor.org/stable/2096992.1986.

Wang, J., Christopher, S. A., Brechtel, F., Kim, J., Schmid, B., Redemann, J., Russell, P. B., Quinn, P., and Holben, B. N.: Geostationary satellite retrievals of aerosol optical thickness during ACE-Asia, J. Geophys. Res., 108, https://doi.org/10.1029/2003JD003580, 2003a.

Wang, J., Christopher, S. A., Reid, J. S., Maring, H., Savoie, D., Holben, B. N., Livingston, J. M., Russell, P. B., and Yang, S.-K.: GOES 8 retrieval of dust aerosol optical thickness over the Atlantic Ocean during PRIDE, J. Geophys. Res., 108, https://doi.org/10.1029/2002JD002494, 2003b.

Wang, Q., Gu, J., and Wang, X.: The impact of Sahara dust on air quality and public health in European countries, Atmospheric Environment, 241, 117771, https://doi.org/10.1016/j.atmosenv.2020.117771, 2020.

Wang, Q., Jacob, D. J., Fisher, J. A., Mao, J., Leibensperger, E. M., Carouge, C. C., Le Sager, P., Kondo, Y., Jimenez, J. L., Cubison, M. J., and Doherty, S. J.: Sources of carbonaceous aerosols and deposited black carbon in the Arctic in winter-spring: implications for radiative forcing, Atmos. Chem. Phys., 11, 12453-12473, 10.5194/acp-11-12453-2011, 2011.

Wang, Q., Saturno, J., Chi, X., Walter, D., Lavric, J. V., Moran-Zuloaga, D., Ditas, F., Pöhlker, C., Brito, J., Carbone, S., Artaxo, P., and Andreae, M. O.: Modeling investigation of light-absorbing aerosols in the Amazon Basin during the wet season, Atmos. Chem. Phys., 16, 14775-14794, 10.5194/acp-16-14775-2016, 2016.

Wang, W., Evan, A. T., Lavaysse, C., and Flamant, C.: The role the Saharan Heat Low plays in dust emission and transport during summertime in North Africa, Aeolian Res., 28, 1-12, https://doi.org/10.1016/j.aeolia.2017.07.001, 2017.

Wang, Y., Jacob, D. J., and Logan, J. A.: Global simulation of tropospheric O3-NO x -hydrocarbon chemistry: 1. Model formulation, J. Geophys. Res. , 103, 10713-10725, https://doi.org/10.1029/98JD00158, 1998.

Wesely, M. L.: Parameterization of surface resistances to gaseous dry deposition in regional-scale numerical models, Atmos. Environ., 41, 52-63, https://doi.org/10.1016/j.atmosenv.2007.10.058, 2007.

White, B. R.: soil transport by winds on Mars, Journal of Geophysical Research: Solid Earth, 84, 4643-4651, https://doi.org/10.1029/JB084iB09p04643, 1979.

Wu, L., Li, X., Kim, H., Geng, H., Godoi, R. H. M., Barbosa, C. G. G., Godoi, A. F. L., Yamamoto, C. I., de Souza, R. A. F., Pöhlker, C., Andreae, M. O., and Ro, C. U.: Single-particle characterization of aerosols collected at a remote site in the Amazonian rainforest and an urban site in Manaus, Brazil, Atmos. Chem. Phys., 19, 1221-1240, 10.5194/acp-19-1221-2019, 2019.

Ysard, N., Jones, A. P., Demyk, K., Boutéraon, T., and Koehler, M.: The optical properties of dust: the effects of composition, size, and structure, A&A, 617, A124, 2018.

Yu, H., Chin, M., Bian, H., Yuan, T., Prospero, J. M., Omar, A. H., Remer, L. A., Winker, D. M., Yang, Y., Zhang, Y., and Zhang, Z.: Quantification of trans-Atlantic dust transport

from seven-year (2007–2013) record of CALIPSO lidar measurements, Remote Sens. Environ., 159, 232-249, https://doi.org/10.1016/j.rse.2014.12.010, 2015a.

Yu, H., Chin, M., Yuan, T., Bian, H., Remer, L. A., Prospero, J. M., Omar, A., Winker, D., Yang, Y., Zhang, Y., Zhang, Z., and Zhao, C.: The fertilizing role of African dust in the Amazon rainforest: A first multiyear assessment based on data from Cloud-Aerosol Lidar and Infrared Pathfinder Satellite Observations, Geophys. Res. Lett., 42, 1984-1991, 10.1002/2015GL063040, 2015b.

Yu, Y., Kalashnikova, O. V., Garay, M. J., Lee, H., Notaro, M., Campbell, J. R., Marquis, J., Ginoux, P., and Okin, G. S.: Disproving the Bodélé Depression as the Primary Source of Dust Fertilizing the Amazon Rainforest, Geophysical Research Letters, 47, 2020.

Yu, H., Tan, Q., Chin, M., Remer, L. A., Kahn, R. A., Bian, H., Kim, D., Zhang, Z., Yuan, T., Omar, A. H., Winker, D. M., Levy, R. C., Kalashnikova, O., Crepeau, L., Capelle, V., and Chédin, A.: Estimates of African Dust Deposition Along the Trans-Atlantic Transit Using the Decadelong Record of Aerosol Measurements from CALIOP, MODIS, MISR, and IASI, J. Geophys. Res., 124, 7975-7996, https://doi.org/10.1029/2019JD030574, 2019.

Yuan, T., Yu, H., Chin, M., Remer, L. A., McGee, D., and Evan, A.: Anthropogenic Decline of African Dust: Insights From the Holocene Records and Beyond, Geophys. Res. Lett., 47, e2020GL089711, https://doi.org/10.1029/2020GL089711, 2020.

Zender, C. S., Bian, H., and Newman, D.: Mineral Dust Entrainment and Deposition (DEAD) model: Description and 1990s dust climatology, J. Geophys. Res., 108, https://doi.org/10.1029/2002JD002775, 2003.

Zhang, L., Gong, S., Padro, J., and Barrie, L.: A size-segregated particle dry deposition scheme for an atmospheric aerosol module, Atmos. Environ., 35, 549-560, https://doi.org/10.1016/S1352-2310(00)00326-5, 2001.

Zhang, L., Kok, J. F., Henze, D. K., Li, Q., and Zhao, C.: Improving simulations of fine dust surface concentrations over the western United States by optimizing the particle size distribution, Geophys. Res. Lett., 40, 3270-3275, 10.1002/grl.50591, 2013.

1270   Table 1. Annual and seasonal dust emissions (Pg a

Table 1. ⁻¹) in northern Africa (17.5° W – 40° E, 10° N – 35° N)ᵃ.

Year	Spring	Summer	Fall	Winter	Annual (Wet season)
2013	1.2	0.77	0.48	1.0	0.88 (1.1)
2014	0.83	0.84	0.51	0.91	0.77 (0.89)
2015	1.2	0.46	0.33	1.1	0.77 (1.3)
2016	0.82	0.52	0.37	0.89	0.65 (0.86)
2017	0.68	0.38	0.47	0.70	0.56 (0.63)
Mean±std[b]	0.95±0.24	0.59±0.20	0.43±0.078	0.92±0.15	0.73±0.12 (0.96±0.25)

ᵃ Spring: March – May; Summer: June – August; Fall: September – November; Winter: January, February, and December; Wet season: January – April

ᵇ standard deviation

Table 2. Mass fractions (%) of dust emitted in each bin for different particle mass size distribution (PMSD) schemes tested in GEOS-Chem.

Scheme	bin 1				bin 2	bin 3	bin 4
	sub-bin 1 $(0.1 - 0.18)^a$ $(3.1)^b$	sub-bin 2 $(0.18 - 0.3)^a$ $(4.3)^b$	sub-bin 3 $(0.3 - 0.6)^a$ $(2.7)^b$	sub-bin 4 $(0.6 - 1.0)^a$ $(0.96)^b$	$(1.0 - 1.8)^a$ $(0.45)^b$	$(1.8 - 3.0)^a$ $(0.27)^b$	$(3.0 - 6.0)^a$ $(0.16)^b$
V12	7.7 / 0.7	3.32	24.87	71.11	19.2	34.9	38.2
V12_C	12.2 / 6	12	24	58.00	25.3	32.2	30.2
V12_F	5.5 / 3.9	8.06	43	45.04	11.9	15.6	67

ᵃ size range in radius (μm) for each bin

ᵇ mass extinction efficiency (MEE) at wavelength of 550 nm in unit of $m^2\ g^{-1}$ for dust particles in each bin in the GEOS-Chem modelmod

Table 2. Summary of the observations used in this study, including the parameters, the spatio-temporal coverage, and the corresponding application in the model.

Datasets	Parameters	Locations	Periods (resolution)	Application
AERONET	AOD	northern Africa, the Atlantic Ocean	2013 – 2017 (daily)	Model AOD evaluation over northern Africa and the Atlantic Ocean

	PVSD[a]	northern Africa	2013 – 2017 (daily)	Model dust PMSD evaluation
Fennec Campaign	PMSD[b]	Over Mali and Algeria, Africa	17 – 28 June, 2011	Model dust PMSD evaluation
MODIS	AOD	northern Africa and the Atlantic Ocean	2013 – 2017 (daily)	Model AOD evaluation over northern Africa and the Atlantic Ocean
Cayenne	PM$_{10}$	52.3097° W, 4.9489° N (France)	January – April, 2014 (daily)	Model dust mass concentration evaluation at the coast of South America
ATTO	PNSD[c]	59.0056° W, 2.1459° S (Brazil)	January – April, 2014 – 2016 (5 min)	Model dust mass concentration evaluation at the central Amazon Basin

[a] particle volume size distribution; [b] particle mass size distribution; [c] particle number size distribution

Table 3. Annual and seasonal dust emissions (Pg yr^{-1}) in northern Africa (17.5° W – 40° E, 10° N – 35° N)[a].

Year	Spring	Summer	Fall	Winter	Annual (Wet season)
2013	1.2	0.77	0.48	1.0	0.88 (1.1)
2014	0.83	0.84	0.51	0.91	0.77 (0.89)
2015	1.2	0.46	0.33	1.1	0.77 (1.3)
2016	0.82	0.52	0.37	0.89	0.65 (0.86)
2017	0.68	0.38	0.47	0.70	0.56 (0.63)
Mean±std[b]	0.95±0.24	0.59±0.20	0.43±0.078	0.92±0.15	0.73±0.12 (0.96±0.25)

[a] Spring: March – May; Summer: June – August; Fall: September – November; Winter: January, February, and December; Wet season: January – April

[b] standard deviation

Table 34. Estimates of annual dust and associated phosphorus deposition into the Amazon Basin.

Methods	Dust deposition		P deposition		References
	total (Tg a^{-1})	flux (g m^{-2} a^{-1})	total (Tg a^{-1})	flux (mg m^{-2} a^{-1})	
CESM2	10 ± 2.1	n/a	0.0077±0.0016	n/a	Li et al. (2021)[a]
AeroCom Phase I	7.7	0.81	0.0063	0.66	Kok et al. (2021)[b]
MERRA-2	8.0	1.05	0.0062	0.9	Prospero et al. (2020)[a]
MERRA-2, CAM	n/a	n/a	0.011 – 0.033	1.1 – 3.5	Barkley et al. (2019)[a]
GLOMAP	32	1.8	0.019	1.1	Herbert et al. (2018)[a]
CALIOP	8– 48	0.8 – 5	0.006 – 0.037	0.7 – 3.9	Yu et al. (2015b)[a]
ECHAM5	30.3/11.4	n/a	0.025/0.0093	n/a	Gläser et al. (2015)[b]
GEOS-Chem	17± 5	n/a	0.014	n/a	Ridley et al. (2012)[b]
MATCH	n/a	n/a	n/a	0.48	Mahowald et al. (2005)[a]
MODIS	50	n/a	0.041	n/a	Kaufman (2005)[b]
Field measurement	13	19	0.011	16	Swap et al. (1992)[b]
GEOS-Chem	10 ± 1.7	1.2 ± 0.20	0.0085 ± 0.0014	0.97 ± 0.16	This study

1302   *Note*. Table extracted in part from Prospero et al. (2020).

1303   [a] The P mass fraction is 0.077% for Li et al. (2021) and Prospero et al. (2020), 0.108% for Barkley

1304   et al. (2019), 0.088% for Herbert et al. (2018), 0.078% for Yu et al. (2015b), and 0.07% for

1305   Mahowald et al. (2005).

1306   [b] Assuming P mass fraction of 0.082% in dust, the same value as used in this study.

1307

1308

1309

1310
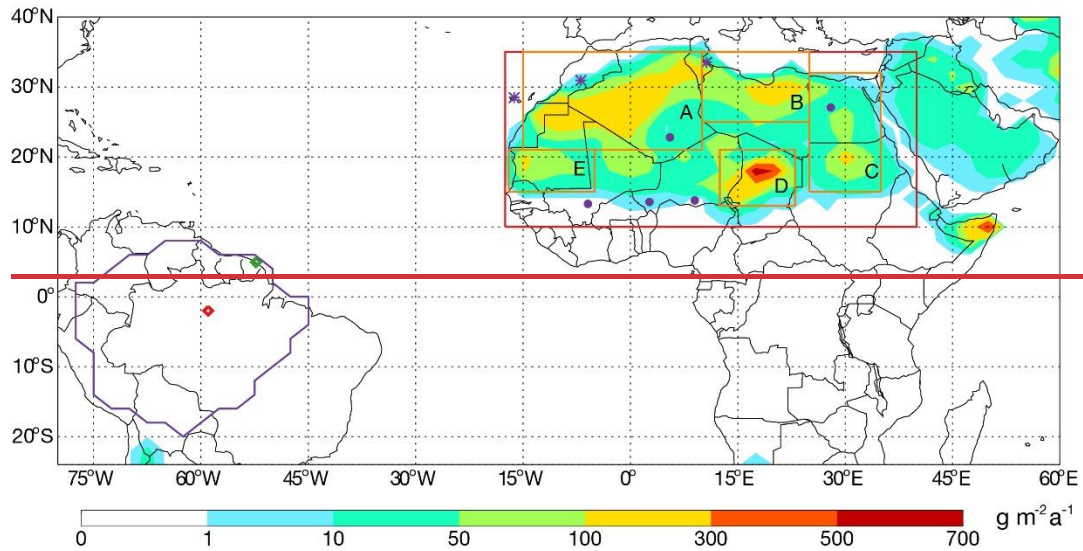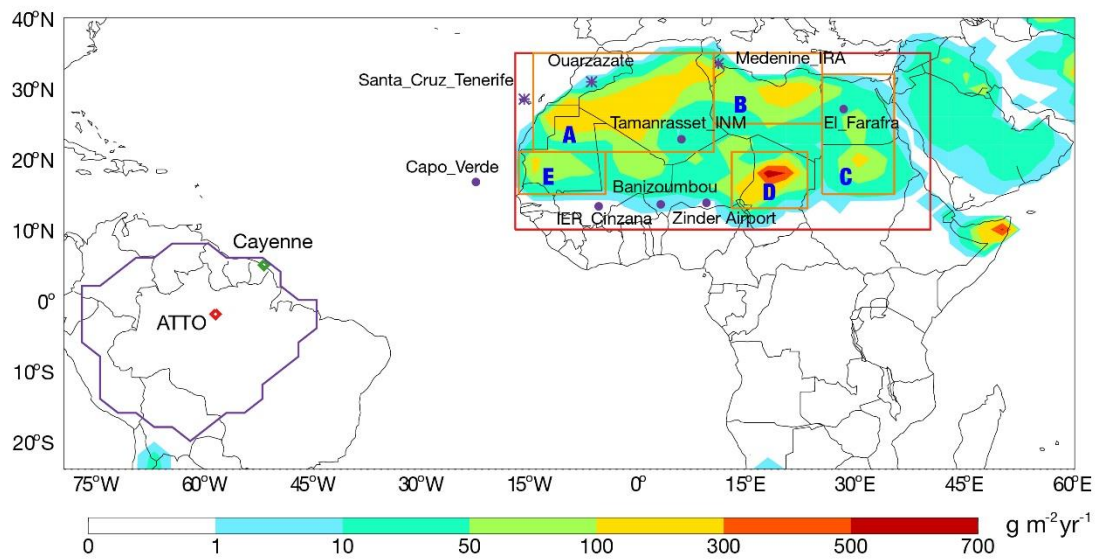
Figure 1. Simulated annual dust emissions in GEOS-Chem, averaged from 2013 to 2017. The location of AERONET sites used in ~~Fig. 3~~Figure 2 are marked as purple symbols, of which circles represent the sites used in ~~Fig. 4~~Figure 3. The region of the Amazon Basin is defined by purple lines. The location of Cayenne site in the northeast coast of South America and ATTO site in the central Amazon Basin are marked as green and red diamonds, respectively. The red rectangle illustrates the area of northern Africa (17.5° W – 40° E, 10° N – 35° N) and the orange rectangles shows the areas of five major source regions described in the text (A: 15° W – 10° E, 21° N – 35° N; B: 10° E – 25° E, 25° N – 35°-N; C: 25° E – 35° E, 15° N – 32° N; D: 12.5° E – 23° E, 13° N – 21° N; E: 17° W – 5°-W, 15° N – 21° N).—

1326
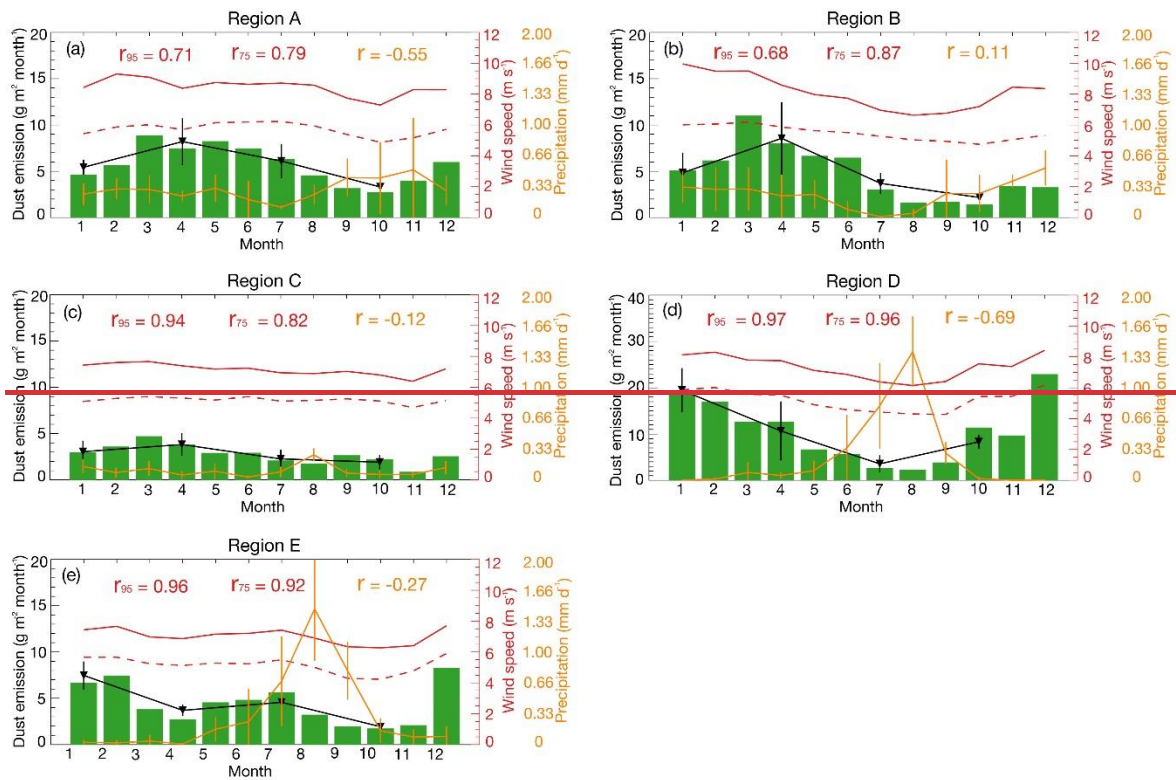
1327

1328 **Figure 2.** ~~Monthly dust emission fluxes together with the 95th percentile hourly wind~~

1329 ~~speeds (red solid lines), the 75th percentile hourly~~ ~~wind speeds (red dotted lines) and~~

1330 ~~precipitation (yellow lines) over the five major source regions averaged from 2013 to 2017. Seasonal~~

1331 ~~emission fluxes of dust are also shown as black lines. The correlation coefficients (r) between the~~

1332 ~~dust emission fluxes and different meteorological variables are also shown in each panel.~~

1333 —

1334 —

1335
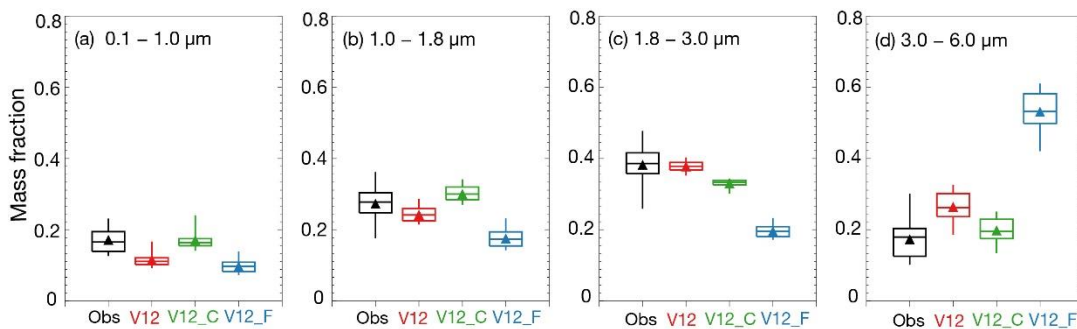
1336 **Figure ~~3~~2.** Boxplots of the mass fractions of column-integrated aerosols in the four size bins (in

1337 radius) retrieved from AERONET sites over Africa compared with model results based on different

1338 PMSD schemes. The triangles represent the mean values.

1339

IER_Cinzana (5.9° W, 13.3° N)

Banizoumbou (2.7° E, 13.5° N)

Zinder_Airport (9.0° E, 13.8° N)

Tamanrasset_INM (5.5° E, 22.8° N)

El_Farafra (28.0° E, 27.1° N)
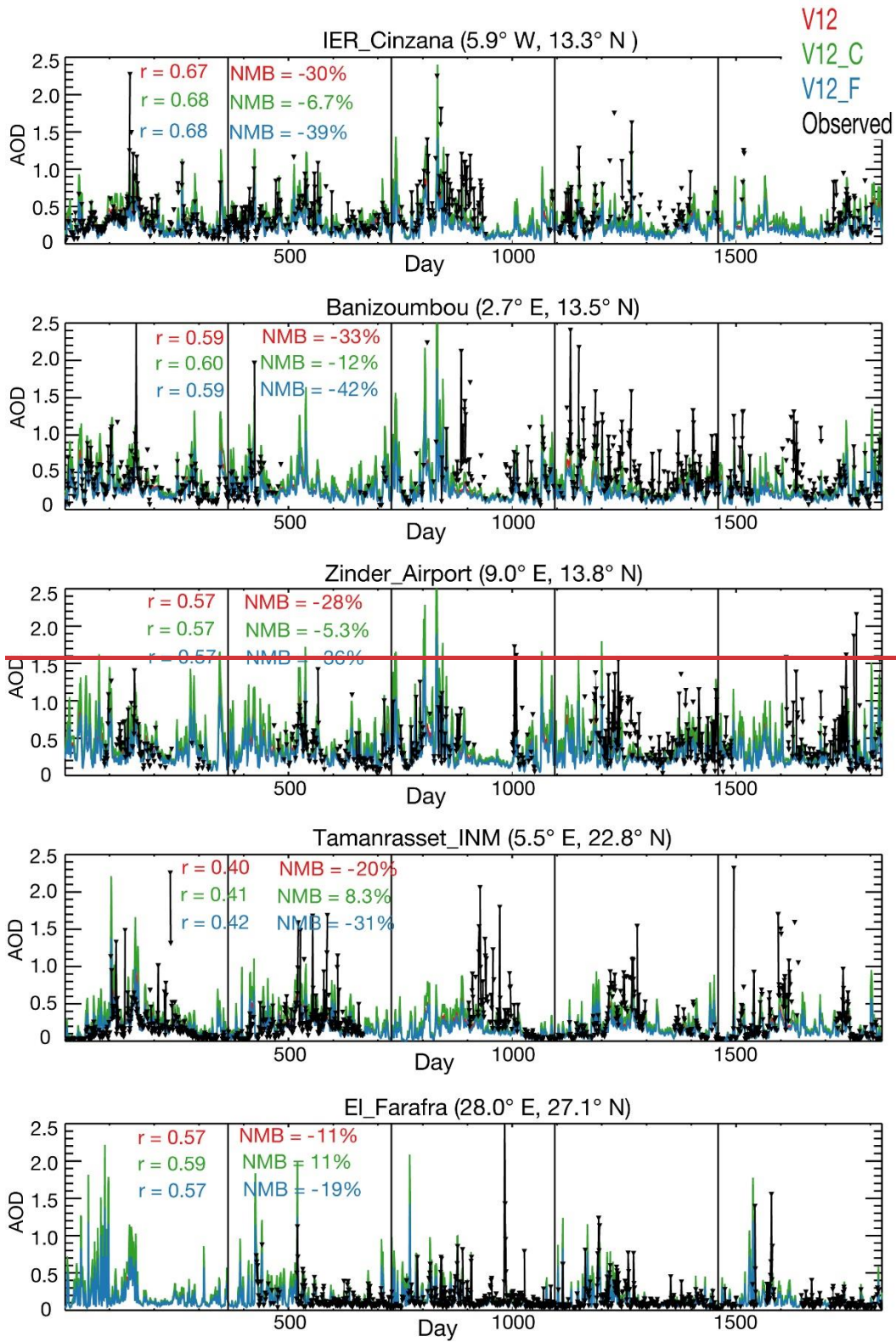
1340
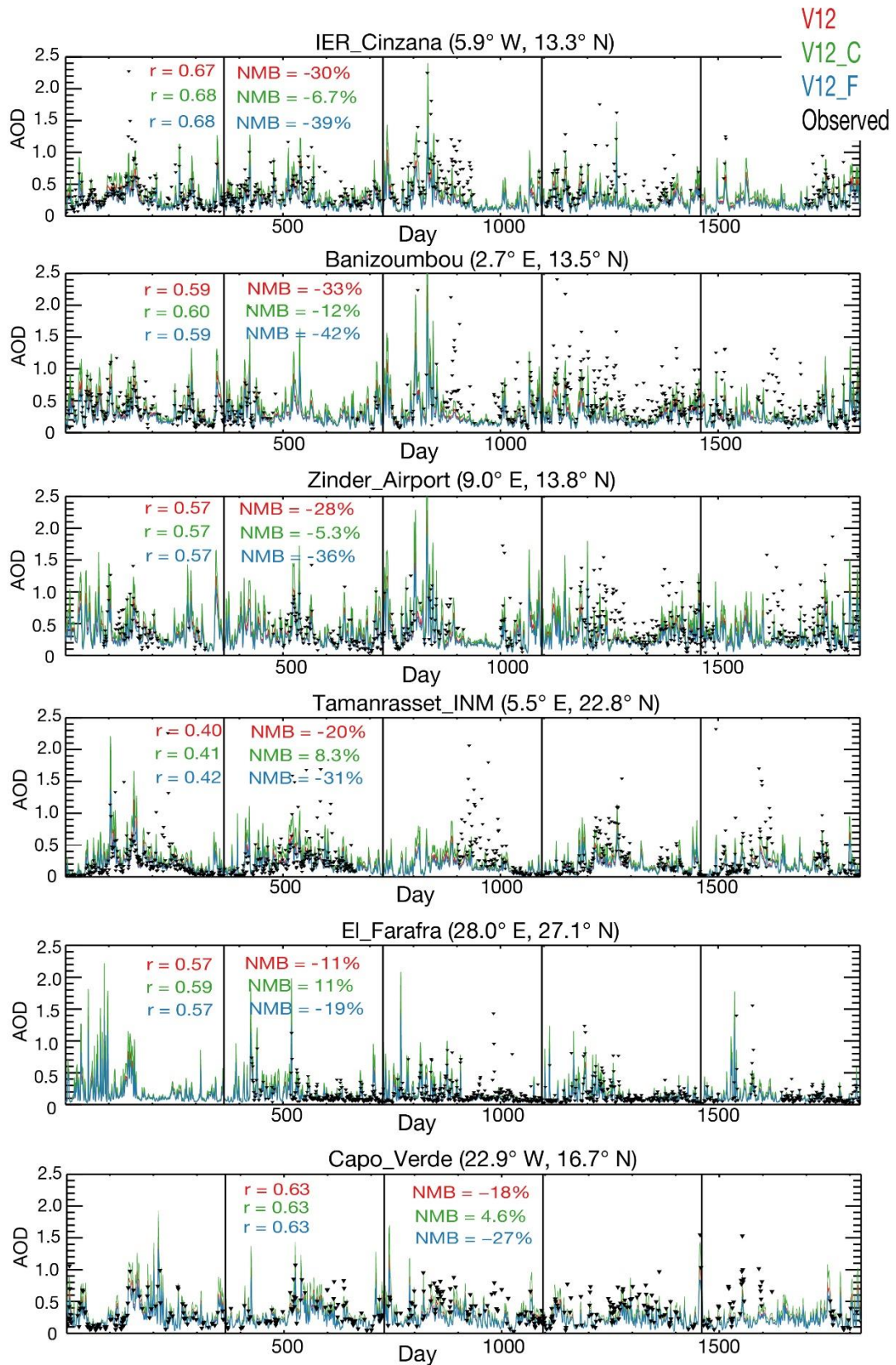
Figure 43. Time series of AERONET (black lines) and simulated daily AOD (at wavelength of 675 nm) during 2013 – 2017. Normalized mean bias (NMB) and correlation (*r*) statistics between the

47

AERONET and simulated data are shown as inset.

48
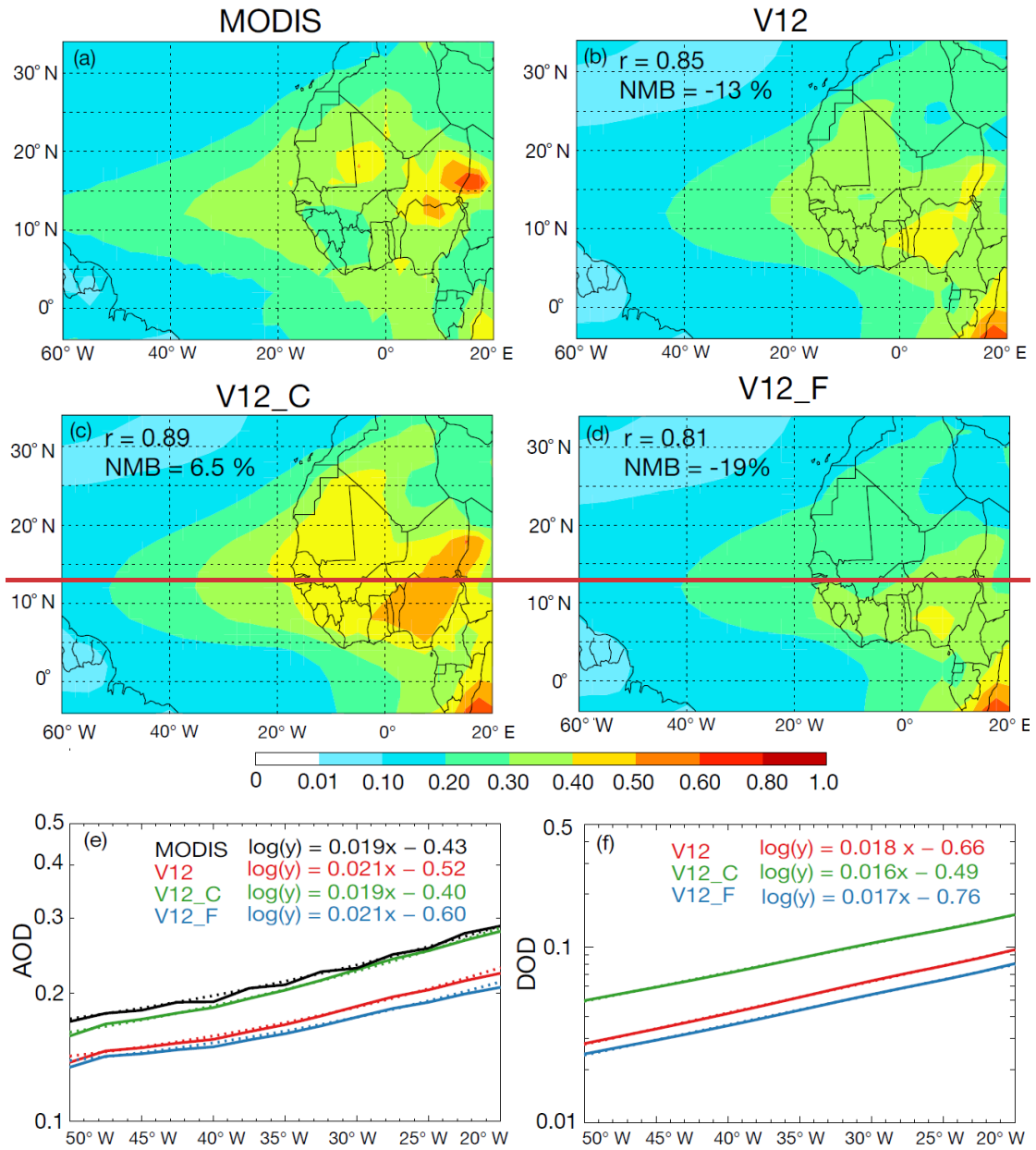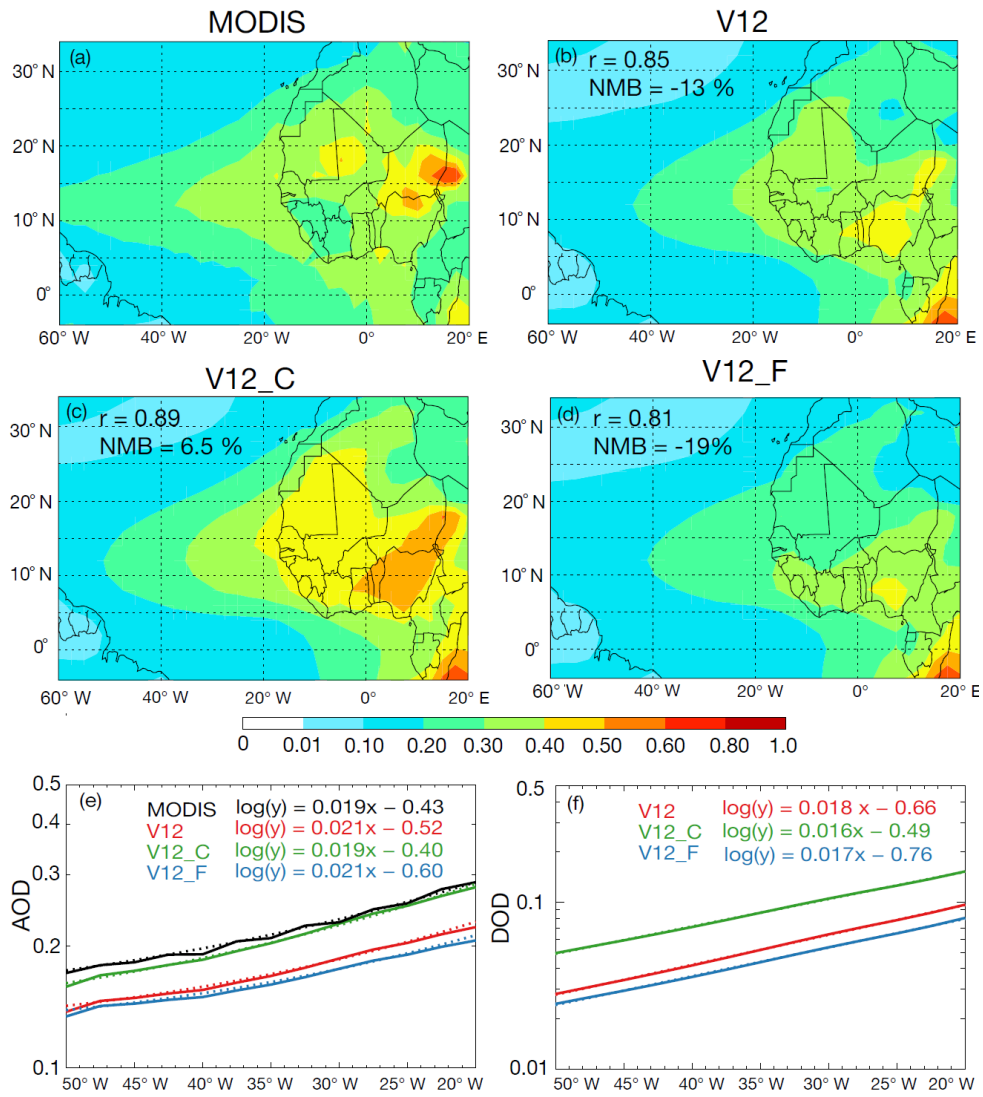
Figure 54. (a) – (d) Spatial distributions of observed and simulated AOD (at 550 nm) over the region of 60° W – 20° E and 10° N – 35° N averaged over 2013 – 2017. Normalized mean bias (NMB) and correlation coefficient (r) between the simulations and MODIS AOD are shown as inset. (e) MODIS (black) and simulated (color) AOD and (f) simulated dust optical depth (DOD) at 550 nm along the transect from 20° to 50° W, averaged over 5° S − 25° N for the period 2013 − 2017. The solid lines represent averaged data and the dashed lines are the logarithmic trend lines.
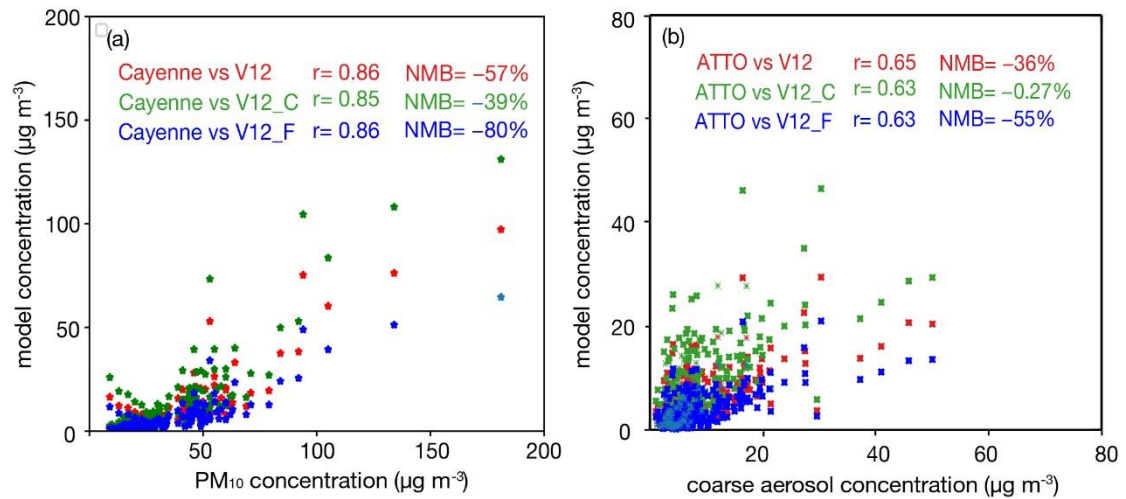
Figure 6~~5~~. Scatter plots of (a) observed PM_{10} and simulated dust concentrations at Cayenne site during wet season of 2014 and (b) observed coarse aerosol (PM_{1-10}) and simulated dust concentrations at ATTO site during wet season of 2014-2016. Normalized mean bias (NMB) and correlation (*r*) statistics between the observation and simulation are shown as inset.
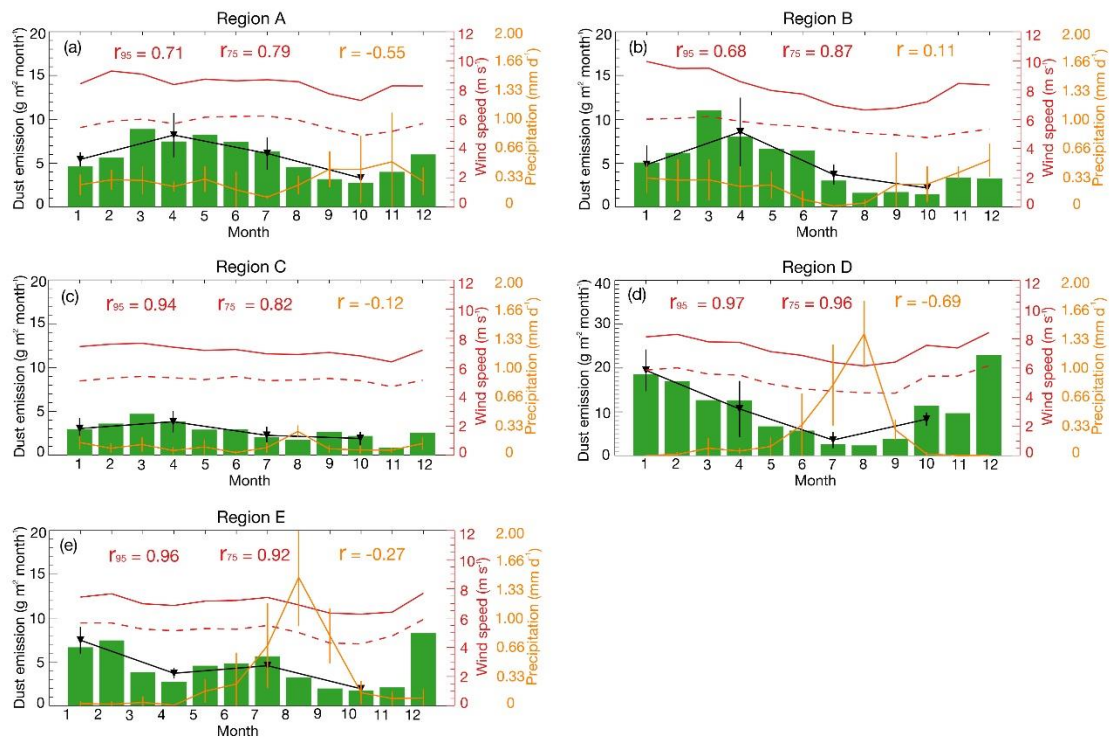
Figure 6. Monthly dust emission fluxes together with the 95th percentile hourly 10-m wind speeds (red solid lines), the 75th percentile hourly 10-m wind speeds (red dotted lines) and precipitation (yellow lines) over the five major source regions averaged from 2013 to 2017. Seasonal emission fluxes of dust are also shown as black lines. The correlation coefficients (r) between the dust emission fluxes and different meteorological variables are also shown in each panel.
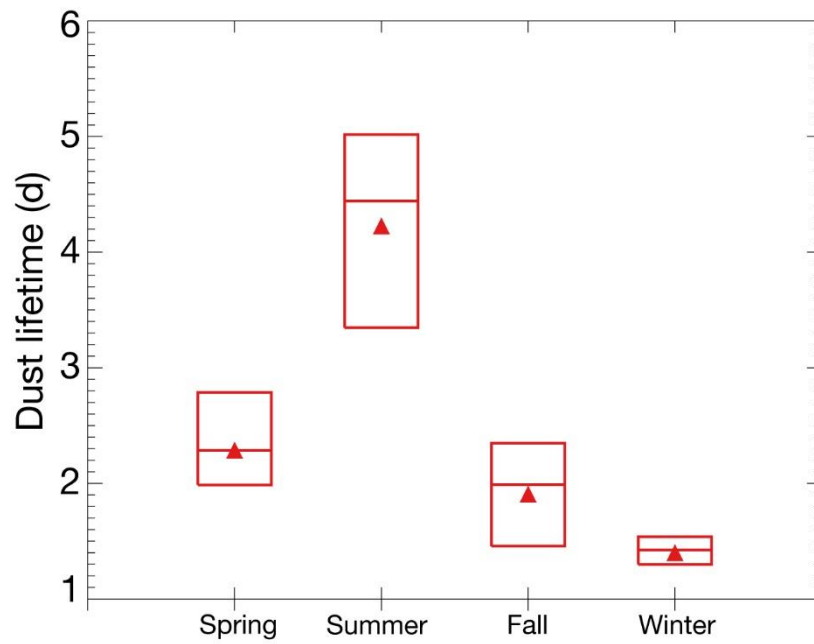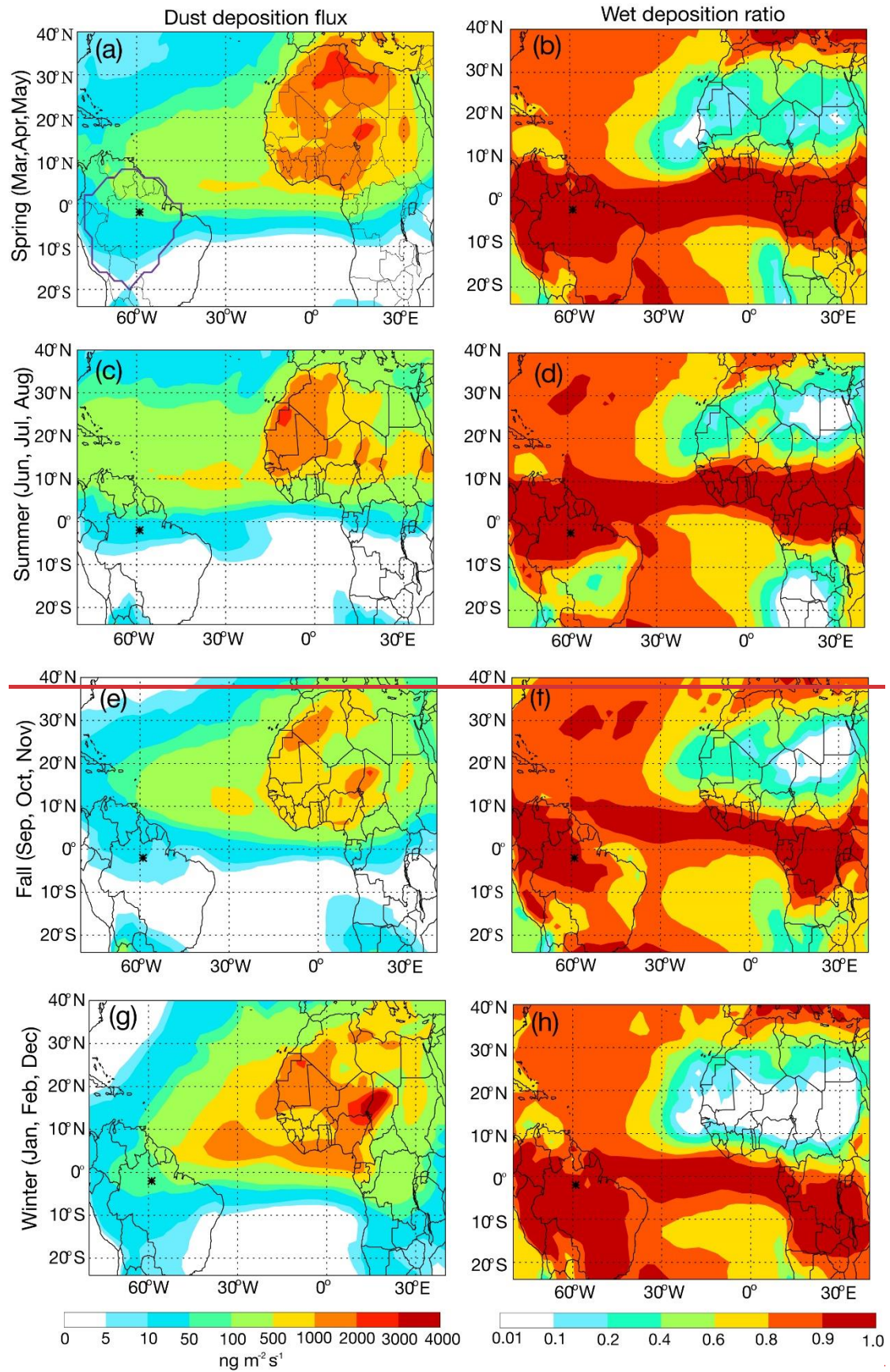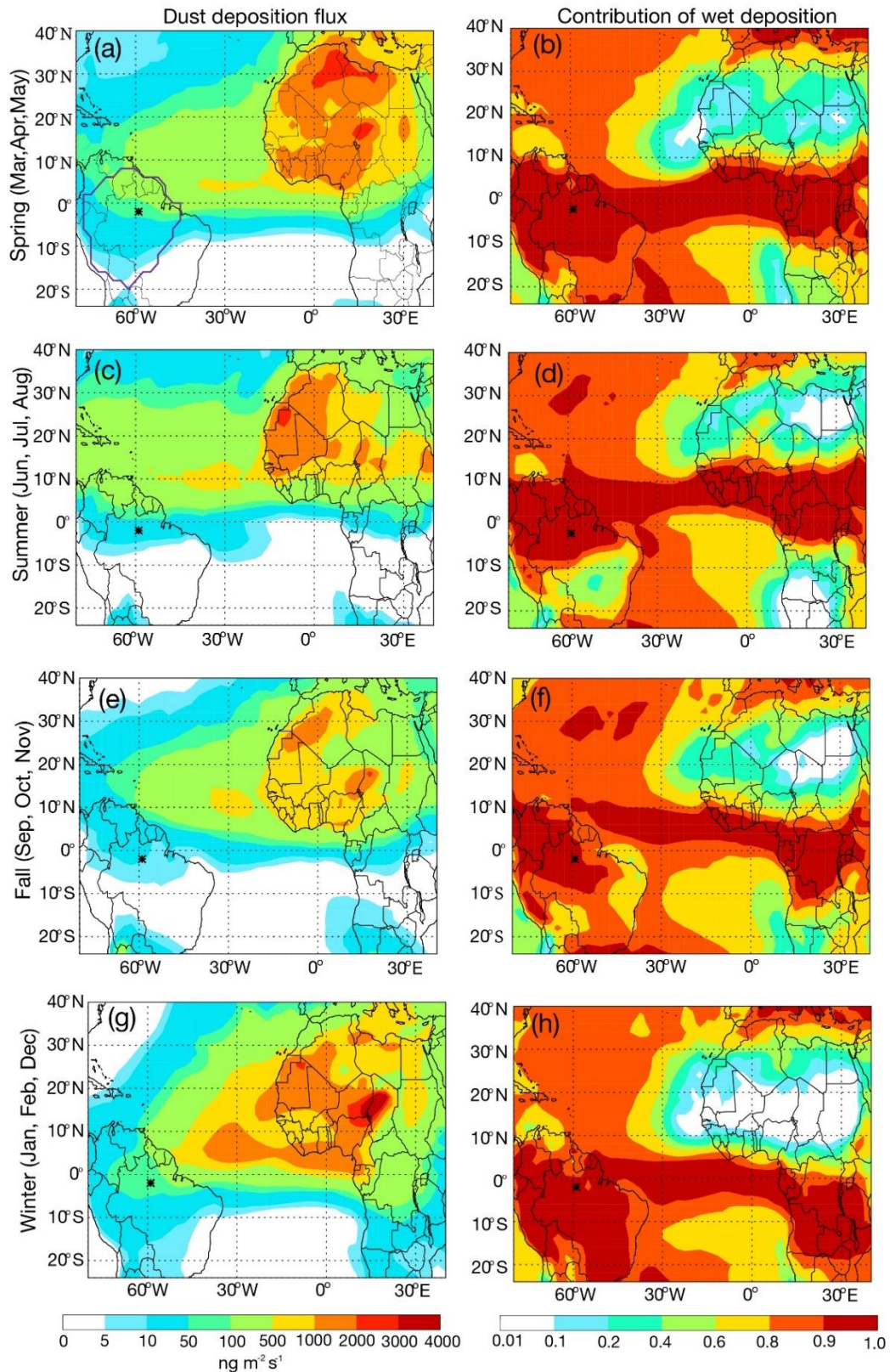
Figure 7. Seasonal e-folding lifetime derived from the logarithm of simulated dust column burden against travel time along the transect from 20° W to 50° W averaged over 5° S − 25° N during the period of 2013 – 2017. The triangles represent the mean values, and the bottom and top sides of the boxes represent the minimums and maximums.
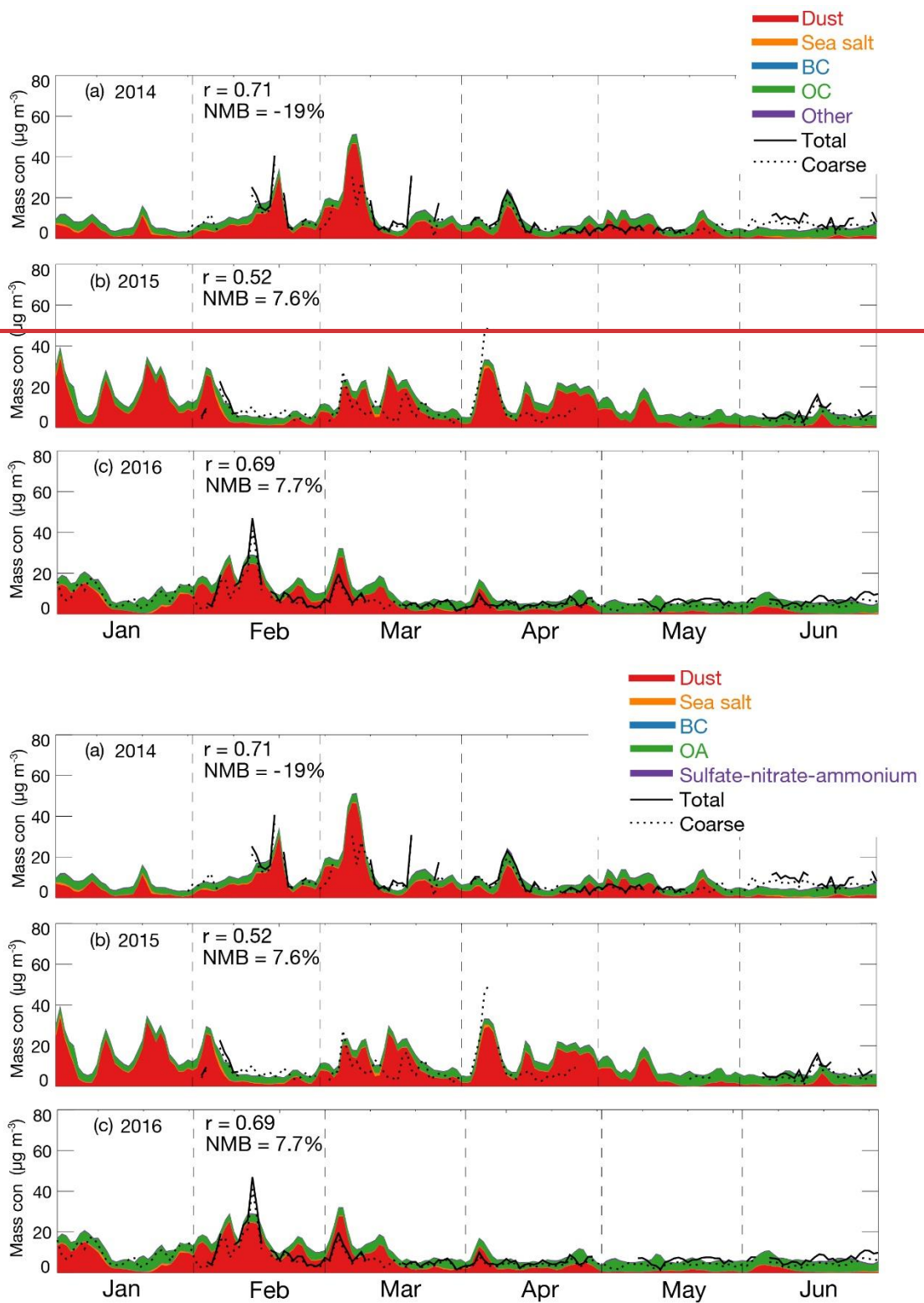
Dust deposition flux

Wet deposition ratio

Figure 8. Simulated seasonal (left) dust deposition fluxes and (right) contribution of wet deposition during 2013-2017. The ATTO site is marked as asterisk. The region of the Amazon Basin is defined by purple lines in ~~Fig. 7a~~Figure 8a.
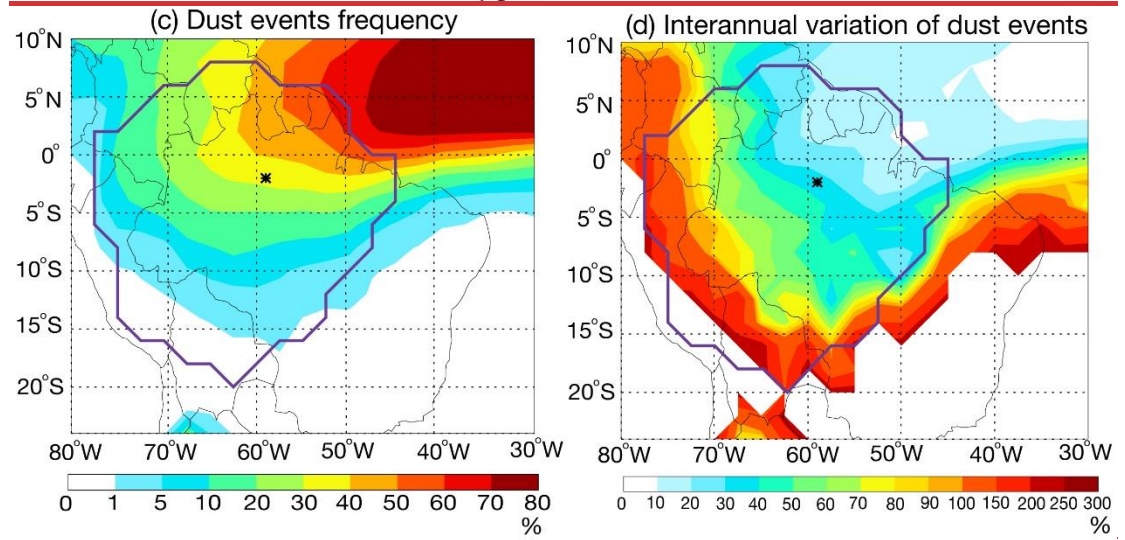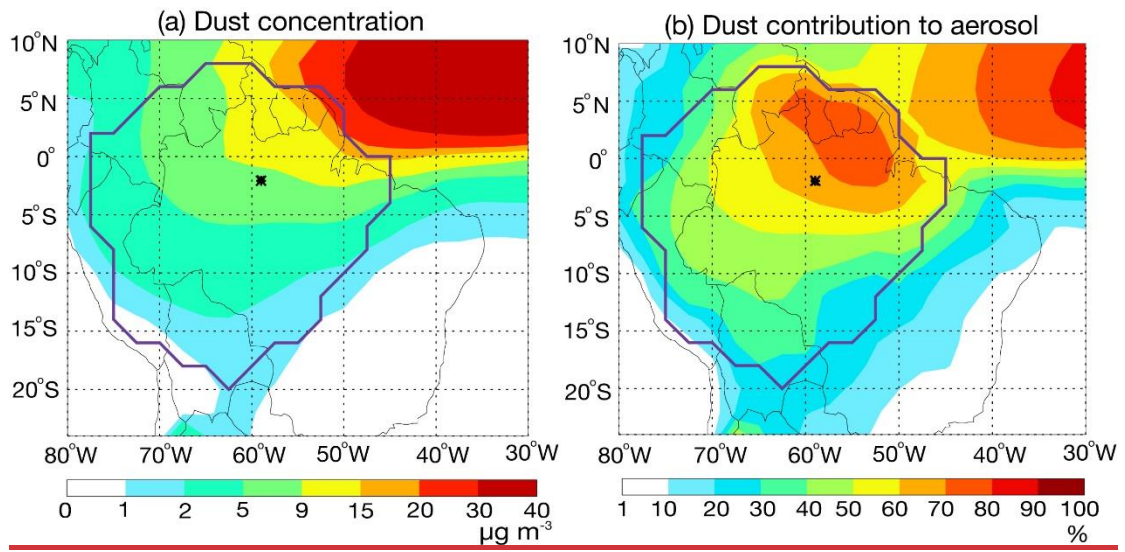
Figure 9. Time series of observed coarse and total aerosol mass concentrations and simulated aerosol species concentrations at the ATTO site from January to June in (a) 2014, (b) 2015, and (c) 2016. Model results are separated into different species shown as stacked areas. Normalized mean bias (NMB) and correlation coefficient (r) between the observed coarse aerosols and simulated dust concentrations are shown as inset.

(a) Dust concentration
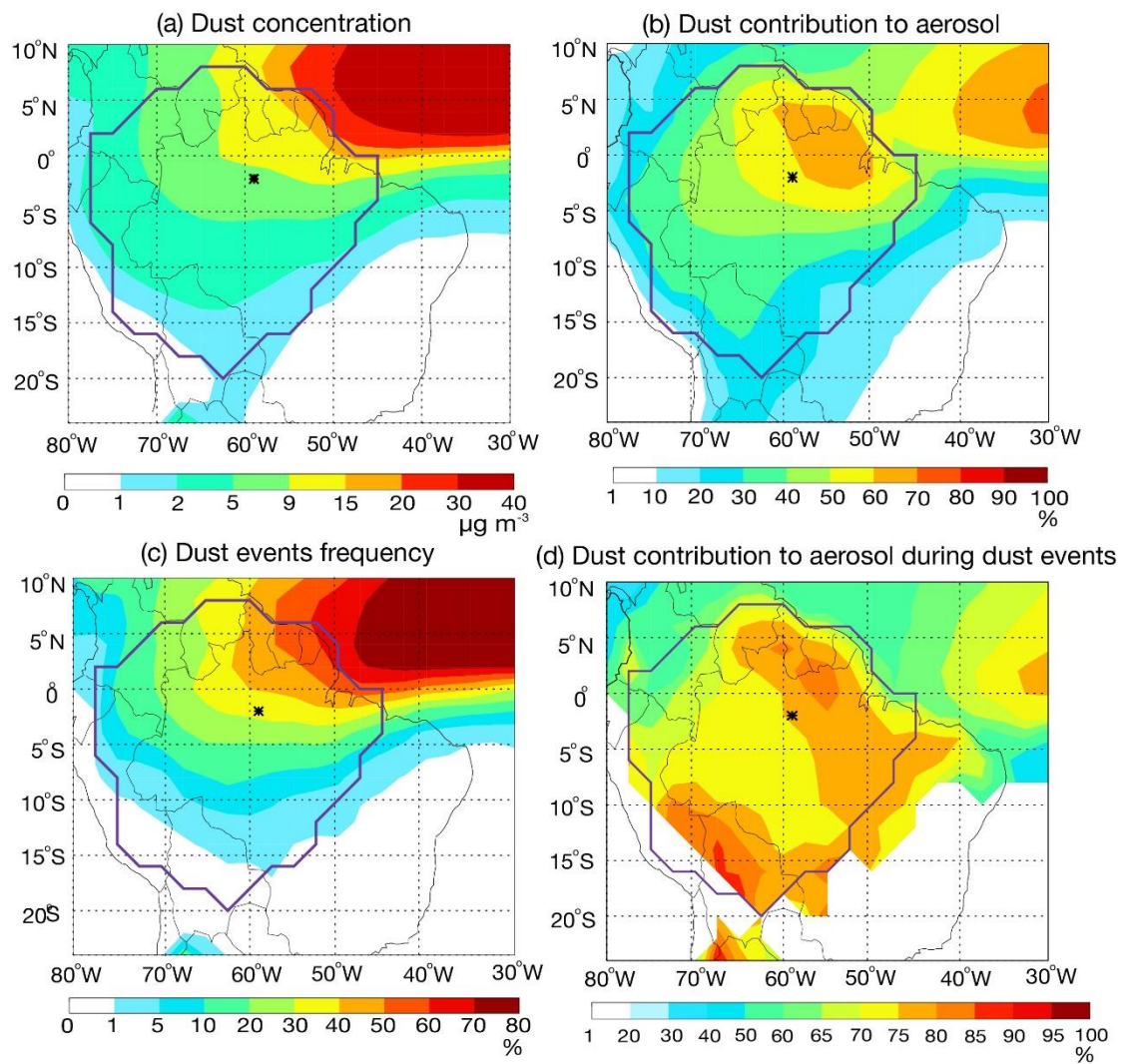
(b) Dust contribution to aerosol

(c) Dust events frequency

(d) Interannual variation of dust events

55

Figure 10. Dust impact over the Amazon Basin in the wet season of 2013 – 2017: (a) simulated surface dust ~~concentration and~~concentrations, (b) ~~its~~dust contribution to surface aerosol ~~concentration over the Amazon Basin in the wet season of 2013-2017.~~concentrations, (c) the frequency of dust events, and (d) ~~its interannual variation (namely relative standard deviation)~~dust contribution to surface aerosol concentrations during ~~the same period~~dust events. The location of ATTO site is marked as asterisks. The region of Amazon Basin is marked by purple lines.
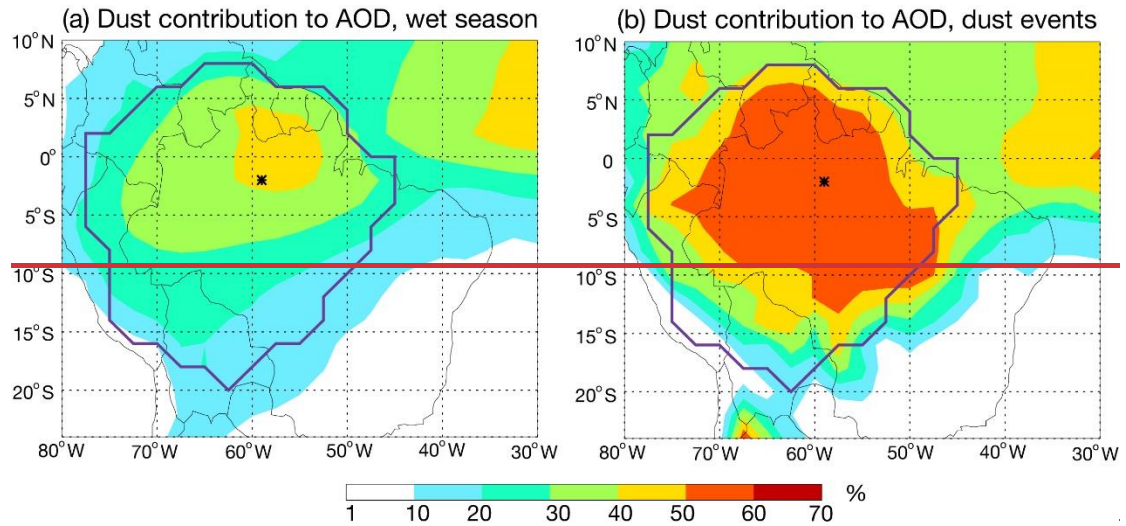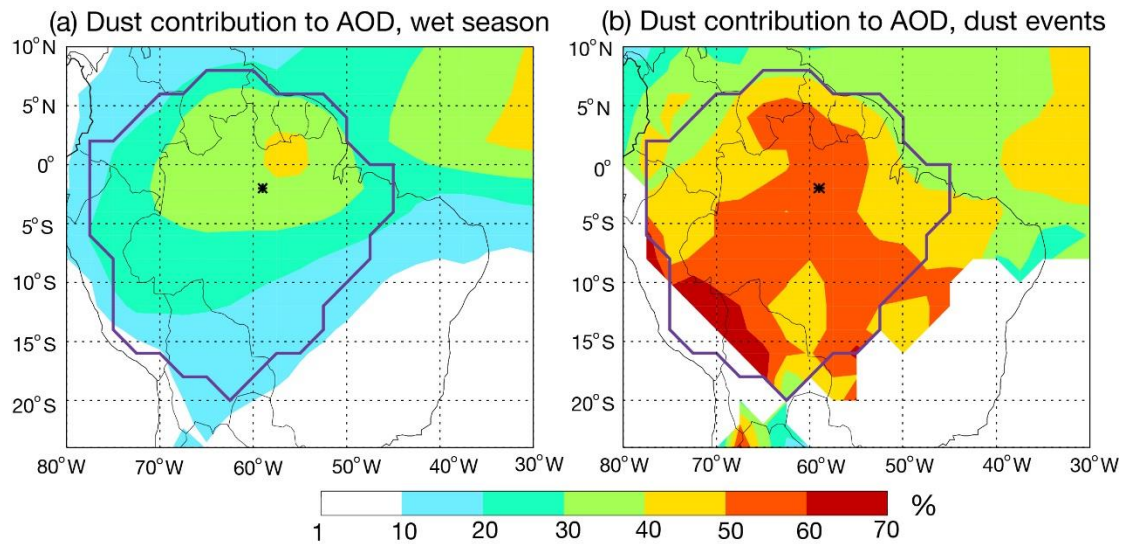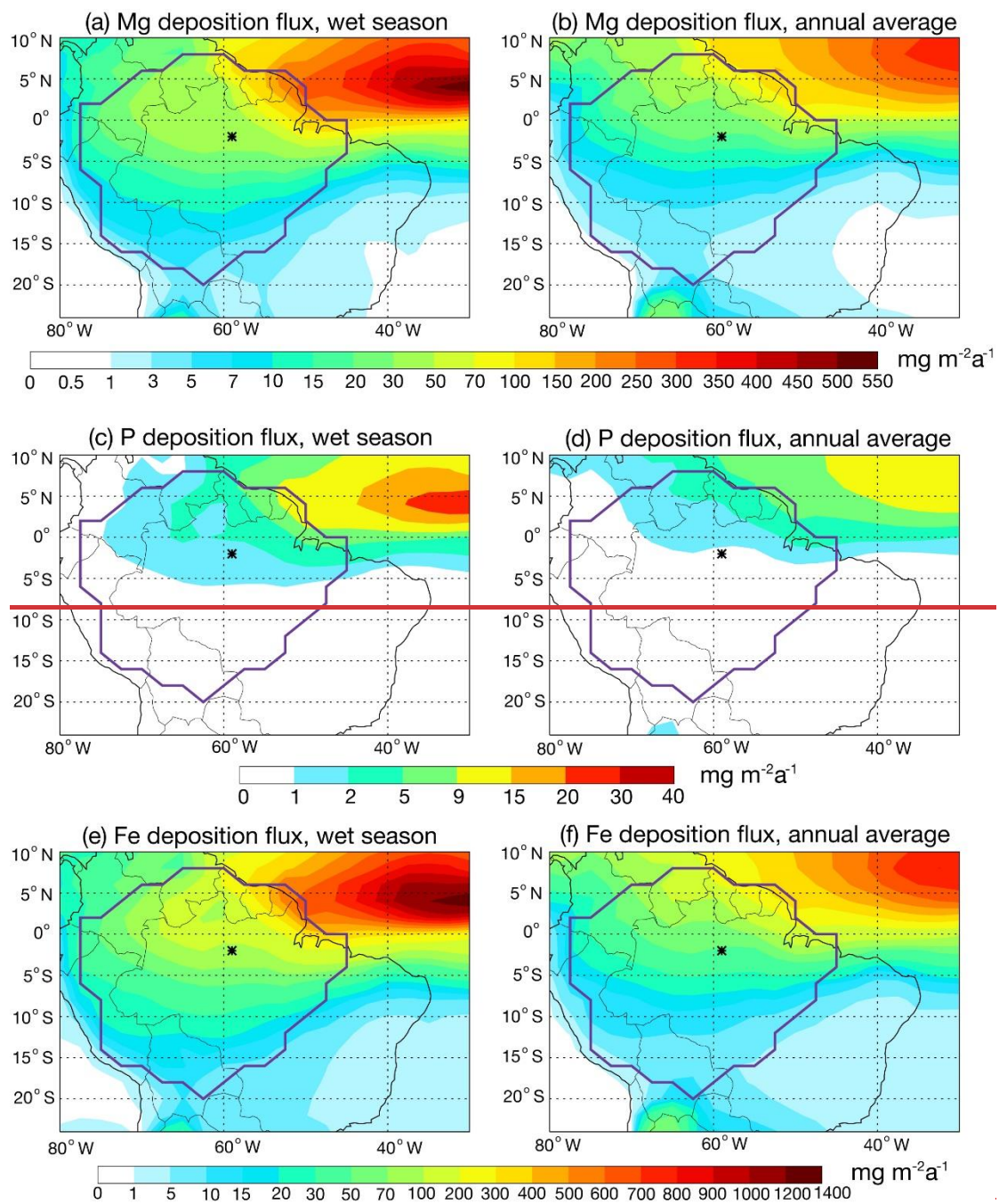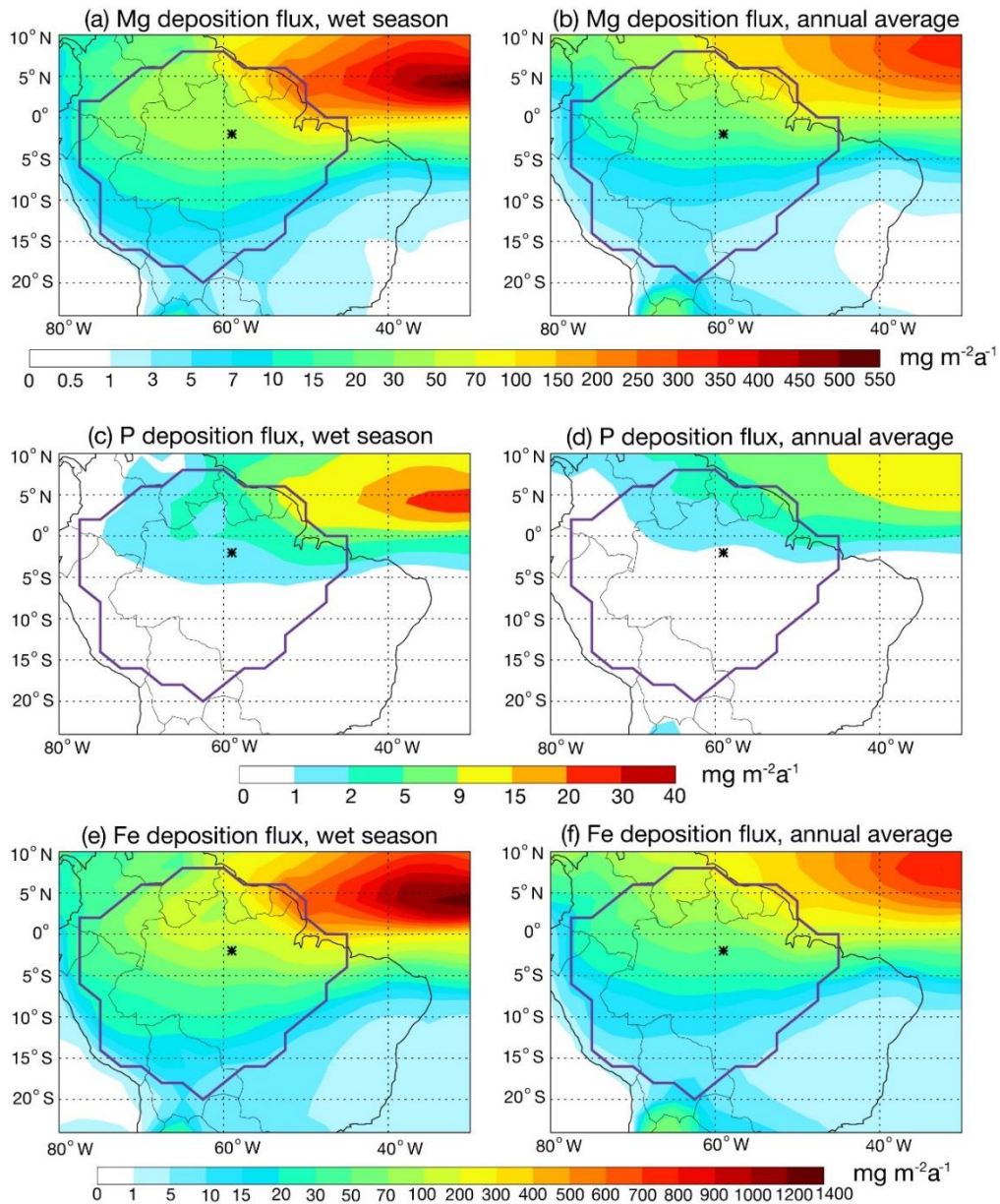
Figure 11. Dust contribution to total AOD at ~~675~~550 nm over the Amazon Basin averaged over the

(a) wet season and (b) dust events during 2013- – 2017. The region of Amazon Basin is marked by

purple lines.

(a) Mg deposition flux, wet season

(b) Mg deposition flux, annual average

mg m^{-2}a^{-1}

0 0.5 1 3 5 7 10 15 20 30 50 70 100 150 200 250 300 350 400 450 500 550

(c) P deposition flux, wet season

(d) P deposition flux, annual average

mg m^{-2}a^{-1}

0 1 2 5 9 15 20 30 40

(e) Fe deposition flux, wet season

(f) Fe deposition flux, annual average

mg m^{-2}a^{-1}

0 1 5 10 15 20 30 50 70 100 200 300 400 500 600 700 800 900 1000 1200 1400

1411

58

Figure 12. Magnesium deposition flux in (a) wet season and (b) annual averaged from 2013 to 2017. Phosphorus deposition flux in (c) wet season and (d) annual averaged from 2013 to 2017. Iron deposition flux in (e) wet season and (f) annual averaged from 2013 to 2017. The location of ATTO site is marked as asterisks. The region of Amazon Basin is marked by purple lines.